Chapter 3

ENERGY LOSSES IN MEMS AND EQUIVALENT VISCOUS DAMPING

3.1 INTRODUCTION

Energy losses change the behavior of mechanical microsystems and limit their performance. The response of a single degree-of-freedom (DOF) mechanical system, for instance, is conditioned by a damping term (force in translatory motion and torque in rotary motion), which can be formulated as a viscous damping agent whose magnitude is proportional to velocity. The damping coefficient is the proportionality constant and various forms of energy losses can be expressed as viscous damping ones, either naturally or by equivalence so that a unitary formulation is obtained. For oscillatory micro/nanoelectro-mechanical systems (MEMS/NEMS), losses can be quantified by means of the quality factor (Q-factor), which is the ratio of the energy stored to the energy lost during one cycle of vibration, and the damping coefficient can be expressed in terms of the Q-factor. Energy losses in MEMS/NEMS are the result of the interaction between external and internal mechanisms. Fluid–structure interaction (manifested as squeeze- or slide-film damping), anchor (connection to substrate) losses, thermoelastic damping (TED), surface/volume losses and phonon-mediated damping are the most common energy loss mechanisms discussed in this chapter.

3.2 LUMPED-PARAMETER VISCOUS DAMPING

3.2.1 Viscous Damping Coefficient and Damping Ratio

Viscous damping in a lumped-parameter system that performs linear motion is expressed by a resistance force, which is proportional to velocity, namely:

$$F_d = c\dot{x} \tag{3.1}$$

where c is the damping coefficient (a similar relationship is obtained for rotary motion where a torque is set through damping resistance and that is proportional to the angular velocity).

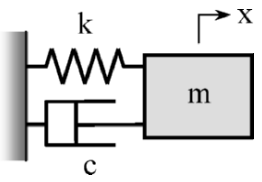

Figure 3.1 Mass-dashpot single DOF system

The damped free vibrations of the single DOF system of Figure 3.1 are described by the equation:

$$m\ddot{x} + c\dot{x} + kx = 0 \tag{3.2}$$

For *linear systems*, the damping coefficient c is constant, as well as the mass m and stiffness k coefficients. However, as shown in the following, situations may appear in damped MEMS/NEMS system where c depends on the vibration frequency (particularly in driven systems). Equation (3.2) in such instances becomes *nonlinear*, and its integration is not pursued in this chapter.

By using the following notations:

$$\begin{cases} \omega_r^2 = \dfrac{k}{m} \\ \zeta = \dfrac{c}{2m\omega_r} \end{cases} \tag{3.3}$$

where ω_r is the resonant frequency and ζ is the *damping ratio*, Equation (3.2) can be rewritten as:

$$\ddot{x} + 2\zeta\omega_r\dot{x} + \omega_r^2 x = 0 \tag{3.4}$$

which is the standard form known from vibrations. There are three different cases and their corresponding solutions depend on the value of the damping ratio ζ. When $0 < \zeta < 1$, which leads to *underdamped* free vibrations, the solution to Equation (3.4) (e.g., see Thomson [1]) is:

$$x(t) = e^{-\zeta\omega_r t}\left[\left(\frac{\zeta}{1-\zeta^2}x(0) + \frac{\dot{x}(0)}{\omega_d}\right)\sin\left(\omega_d t\right) + x(0)\cos\left(\omega_d t\right)\right] \tag{3.5}$$

where ω_d is the damped resonant frequency and is defined as:

$$\omega_d = \sqrt{1-\zeta^2}\,\omega_r \tag{3.6}$$

Equation (3.5) can be rewritten as:

$$x(t) = Xe^{-\zeta\omega_r t}\sin\left(\omega_d t + \varphi\right) \tag{3.7}$$

where:

$$\begin{cases} X = \dfrac{\dfrac{\zeta}{1-\zeta^2}x(0) + \dfrac{\dot{x}(0)}{\omega_d}}{\cos\varphi} \\ \varphi = \tan^{-1}\dfrac{1}{\dfrac{\zeta}{1-\zeta^2} + \dfrac{\dot{x}(0)}{\omega_d x(0)}} \end{cases} \tag{3.8}$$

For $\zeta = 1$, the vibrations of the system shown in Figure 3.1 are *critically damped* and the solution to Equation (3.4) is:

$$x(t) = e^{-\zeta\omega_r t}\left[x(0)\left(1+\omega_r t\right) + \dot{x}(0)t\right] \tag{3.9}$$

The *overdamped* vibrations occur when $\zeta > 1$, and the solution to Equation (3.4) is in that case:

$$x(t) = ae^{-\left(\zeta+\sqrt{\zeta^2-1}\right)\omega_r t} + be^{-\left(\zeta-\sqrt{\zeta^2-1}\right)\omega_r t} \tag{3.10}$$

with:

$$\begin{cases} a = \dfrac{-\zeta+\sqrt{\zeta^2-1}}{2\sqrt{\zeta^2-1}}x(0) - \dfrac{\dot{x}(0)}{2\omega_r\sqrt{\zeta^2-1}} \\ b = \dfrac{\zeta+\sqrt{\zeta^2-1}}{2\sqrt{\zeta^2-1}}x(0) + \dfrac{\dot{x}(0)}{2\omega_r\sqrt{\zeta^2-1}} \end{cases} \tag{3.11}$$

Figure 3.2 plots the three damped vibration cases under zero initial displacement and non-zero initial velocity. An exponentially decaying envelope is the asymptote curve to the underdamped response curve. The overdamped response curve is rapidly decaying. The critically damped response shows no harmonicity, as well as the overdamped one, and they both rapidly converge towards zero.

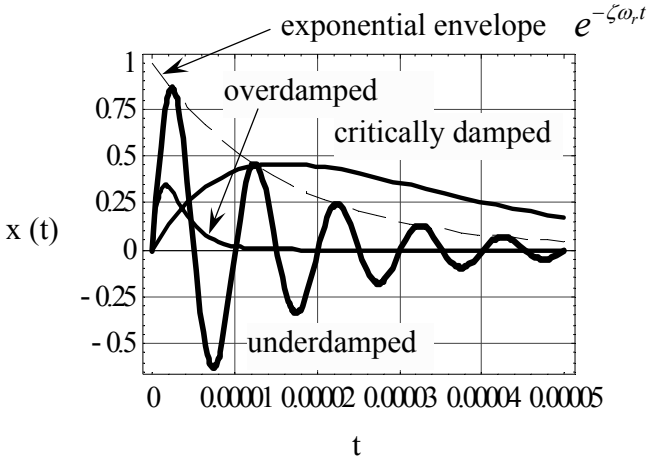

Figure 3.2 Free damped response of underdamped, overdamped, and critically damped single DOF system

3.2.2 Complex Number Representation of Vectors

It is convenient in many situations where harmonic excitation and response are in place to use the complex number representation of vectors. Figure 3.3 shows the one-to-one mapping that connects the classical representation of a vector and the one utilizing complex numbers. Considering the rod in Figure 3.3 rotates at constant angular velocity ω, the projections of point P on the Cartesian frame axes are:

$$\begin{cases} x = R\cos(\omega t) \\ y = R\sin(\omega t) \end{cases} \tag{3.12}$$

because the angle that positions the rotating vector is $\theta = \omega t$ (ω being the constant angular speed).
The velocity components are the time derivatives of x and y of Equation (3.12), and therefore the total velocity is:

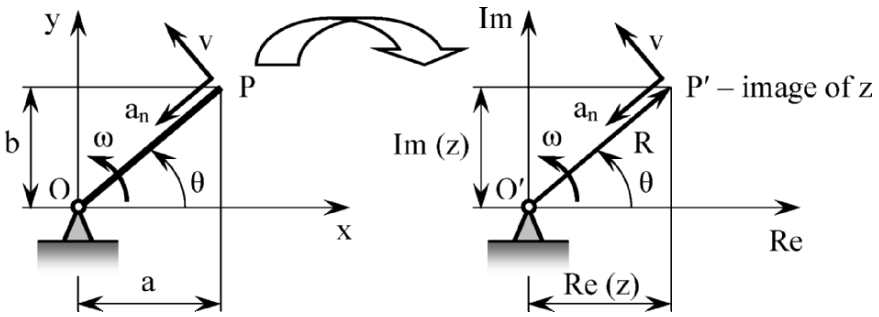

Figure 3.3 Classical planar representation of a vector versus complex-number representation of the same vector

$$v = \sqrt{v_x^2 + v_y^2} = \sqrt{\left(\frac{dx}{dt}\right)^2 + \left(\frac{dy}{dt}\right)^2} = \omega R \tag{3.13}$$

Similarly, the normal acceleration is found by using the *x*- and *y*-components and its well-known value is:

$$a_n = \sqrt{a_x^2 + a_y^2} = \omega^2 R \tag{3.14}$$

The one-to-one mapping of the rotating vector of Figure 3.3 into the complex number representation is warranted by the fact that a complex number is defined by a real component and an imaginary one. When the *x*- and *y*-projections of a vector are identical to the real and imaginary parts of a complex number, respectively, a vector in a plane is mapped into the image of a complex number in the complex plane. The complex number that is the map of the rotating vector in Figure 3.3 can be expressed in algebraic form, as well as in trigonometric and exponential forms (the latter due to Euler's formula), namely:

$$z = x + jy = R\left[\cos(\omega t) + j\sin(\omega t)\right] = Re^{j\omega t} \tag{3.15}$$

The exponential form of a complex number is compact and is used in problems involving harmonic amounts. A few properties of exponential-form complex numbers are illustrated next. Multiplying two complex numbers, namely:

$$z_1 z_2 = R_1 e^{j\theta_1} R_2 e^{j\theta_2} = R_1 R_2 e^{j(\theta_1+\theta_2)} \tag{3.16}$$

indicates the result is another complex number (vector) positioned at $\theta_1 + \theta_2$ and having a magnitude equal to the product of the two multiplying complex numbers. Also, multiplication by the imaginary number j results in:

$$jz = \left(\cos\frac{\pi}{2} + j\sin\frac{\pi}{2}\right) Re^{j\theta} = R\, e^{j\left(\theta+\frac{\pi}{2}\right)} \tag{3.17}$$

which shows the result is the original complex number z rotated by $\pi/2$ clockwise. Similarly, division by j rotates a complex number by $-\pi/2$ (or counterclockwise) because:

$$\frac{z}{j} = -jz = \left(\cos\frac{3\pi}{2} + j\sin\frac{3\pi}{2}\right) R\, e^{j\theta} = R\, e^{j\left(\theta+\frac{3\pi}{2}\right)} = R\, e^{j\left(\theta-\frac{\pi}{2}\right)} \tag{3.18}$$

The velocity and acceleration of point P′ in the complex plane are found by taking the first and second time derivative of z, namely:

$$\begin{cases} v = \dfrac{dz}{dt} = i\omega e^{j\omega t} = j\omega z \\ a_n = \dfrac{d^2 z}{dt^2} = \dfrac{dv}{dt} = -\omega^2 e^{j\omega t} = -\omega^2 z \end{cases} \tag{3.19}$$

The first Equation (3.19) indicates the velocity vector is rotated $\pi/2$ in a clockwise direction with respect to the position vector R (Figure 3.3), whereas the normal acceleration is parallel to the displacement vector but has an opposite direction—both situations being well known properties of the constant angular velocity rotation.

3.2.3 *Q*-Factor

The Q-factor is a figure of merit that takes into consideration the various energy losses in a vibrating system. For an oscillator, it is generally defined as:

$$Q = 2\pi \frac{U_s}{U_d} \tag{3.20}$$

where U_s is the energy stored (in the absence of losses) and U_d is the energy dissipated during one oscillatory cycle.

For a single DOF mechanical system, as the one shown in Figure 3.1, the energy stored in an oscillatory cycle (when damping the energy loss source is disregarded) is due to the elastic spring and is expressed as:

$$U_s = \frac{1}{2} kX^2 \tag{3.21}$$

Considering the work done by the viscous damping force is fully converted into energy lost during one oscillatory cycle, and considering a linear system, as the one shown in Figure 3.1, the damping energy is computed as:

$$U_d = \int F_d dx = c \int \dot{x} dx \tag{3.22}$$

The *Q*-factor is formulated by considering the interaction between the vibratory system and a harmonic (sine or cosine) excitation, and in such a characterization, the *Q*-factor is a forced-response one. The damping of a system can also be judged based on the free response, which would remove any dependency on excitation. Both ways are briefly discussed next.

3.2.3.1 Forced-Response *Q*-Factor

When a sinusoidal force acts on the mass-dashpot system pictured in Figure 3.1, the solution is obtained by carrying out the integration of Equation (3.22) for one period, and the energy lost through damping during one oscillation cycle is:

$$U_d = \pi c \omega X^2 \tag{3.23}$$

Consequently, the *Q*-factor defined in Equation (3.20) becomes:

$$Q = \frac{k}{c\omega} = \frac{1}{2\beta\zeta} \tag{3.24}$$

where $\beta = \omega/\omega_r$. At resonance ($\omega = \omega_r$ and $\beta = 1$), the *Q*-factor reduces to:

$$Q_r = \frac{k}{c\omega_r} = \frac{1}{2\zeta} \tag{3.25}$$

Example 3.1

Analyze the *Q*-factor corresponding to the underdamped translational vibrations of a micromechanical system modeled as a single DOF system under sinusoidal excitation.

Solution:

Equation (3.41) is used for the plot of Figure 3.4 (a), whereas the plot of Figure 3.4 (b) is drawn based on Equation (3.25). Increasing the actuation frequency (which amounts to increasing β) and the damping ratio ζ results in smaller Q-factors (Figure 3.4 (a)). Similarly, by increasing the damping ratio, the Q-factor diminishes (Figure 3.4 (b)).

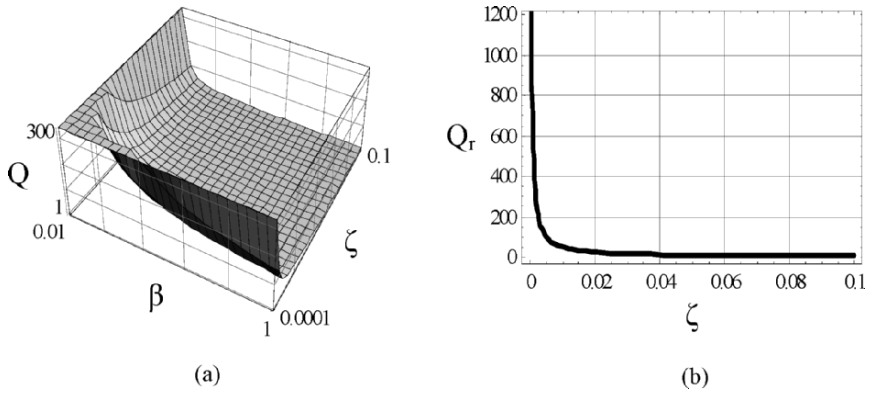

Figure 3.4 Quality factors: (a) regular quality factor; (b) resonant quality factor

Example 3.2

Demonstrate that for a freely damped single DOF vibratory system the Q-factor can be defined as the number of oscillations required to reduce the system's energy to $1/e^{2\pi}$ (approximately 1/535) of its original energy.

Solution:

According to Equation (3.7), the maximum displacement is obtained as:

$$x_{\max}(t) = Xe^{-\zeta\omega_r t} \tag{3.26}$$

If the energy of the system is the one stored in the spring, namely:

$$U = \frac{1}{2}kx_{\max}^2 \tag{3.27}$$

and if n was the number of oscillations necessary to reduce the initial energy to the proportion mentioned in the problem, it means that:

$$\frac{U_0}{U} = \frac{1}{e^{-2\zeta\omega_r nT_r}} = e^{4\pi\zeta n} \tag{3.28}$$

where it has been considered that time t is expressed as:

$$t = nT_r \tag{3.29}$$

and the initial time is $t_0 = 0$. The relationship between the resonant period T_r and circular resonant frequency has also been considered:

$$T_r = \frac{2\pi}{\omega_r} \tag{3.30}$$

The problem's condition is:

$$\frac{U_0}{U} = e^{2\pi} \tag{3.31}$$

Comparing Equations (3.28) and (3.31) yields:

$$n = \frac{1}{2\varsigma} = Q_r \tag{3.32}$$

which demonstrates the problem assertion.

Free decaying underdamped vibrations can be evaluated by means of the *logarithmic decrement* δ, which is defined as the natural logarithm of the ratio of any two successive amplitudes, and, according to Equation (3.7), can be calculated as:

$$\delta = \ln\frac{x_n}{x_{n+1}} = \ln\frac{e^{-\zeta\omega_r nT}}{e^{-\zeta\omega_r (n+1)T}} = \zeta\omega_r T \tag{3.33}$$

By taking into account Equation (3.6), which gives the relationship between the undamped and damped resonant frequencies, Equation (3.33) changes to:

$$\delta = \frac{2\pi\zeta}{\sqrt{1-\zeta^2}} \tag{3.34}$$

When using Equation (3.25), which expresses the resonant Q-factor in terms of the damping ratio, in conjunction with Equation (3.34), the resonant Q-factor results:

$$Q_r = \frac{1}{2}\sqrt{1+4\frac{\pi^2}{\delta^2}} \tag{3.35}$$

Example 3.3

Determine the resonant Q-factor of a nano cantilever whose amplitude decays to $1/e^n$ after m free oscillations. Also determine the equivalent viscous damping.

Solution:

Considering that:

$$\frac{x_1}{x_m} = \frac{x_1}{x_2}\frac{x_2}{x_3}\cdots\frac{x_{m-2}}{x_{m-1}}\frac{x_{m-1}}{x_m} \tag{3.36}$$

the natural logarithm of this relationship is applied, namely:

$$\ln\frac{x_1}{x_m} = \ln\frac{x_1}{x_2} + \ln\frac{x_2}{x_3} + \cdots + \ln\frac{x_{m-2}}{x_{m-1}} + \ln\frac{x_{m-1}}{x_m} = (m-1)\delta \tag{3.37}$$

The problem statement is:

$$\frac{x_1}{x_m} = e^n \tag{3.38}$$

or

$$\ln\frac{x_1}{x_m} = n \tag{3.39}$$

Comparing Equations (3.37) and (3.39) results in:

$$\delta = \frac{n}{m-1} \tag{3.40}$$

The resonant Q-factor becomes, by means of Equations (3.35) and (3.40):

$$Q_r = \frac{1}{2}\sqrt{1+\frac{4\pi^2(m-1)^2}{n^2}} \tag{3.41}$$

Figure 3.5 is the plot of Q_r as a function of m and n.

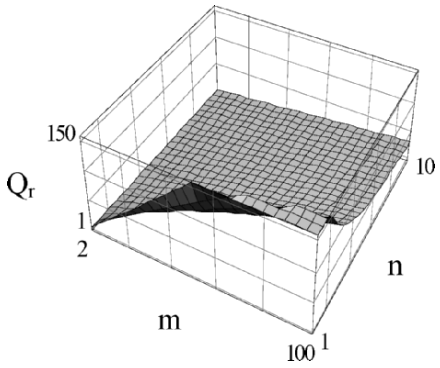

Figure 3.5 Resonant quality factor in terms of the number of cycles and amplitude ratio

Example 3.4

Consider the case in which several loss mechanisms act simultaneously on a MEMS, and that their individual Q-factors are known. Determine the total equivalent Q-factor, the corresponding equivalent damping ratio, as well as the resonant damping ratio, if the individual loss contribution superimpose linearly.

Solution:

The inverse of the Q-factor, as defined in Equation (3.20), is:

$$Q^{-1} = \frac{U_d}{2\pi U_s} \tag{3.42}$$

When several dissipation mechanisms are simultaneously present, the total loss energy can be expressed as:

$$U_d = \sum_i U_{d,i} \tag{3.43}$$

where $U_{d,i}$ are individual loss energy terms. Combination of Equations (3.42) and (3.43) results in:

$$Q_{eq}^{-1} = \frac{\sum_i U_{d,i}}{2\pi U_s} = \sum_i \left(\frac{U_{d,i}}{2\pi U_s} \right) = \sum_i Q_i^{-1} \tag{3.44}$$

In other words, the inverse of the total Q-factor is the sum of the individual Q-factor inverses. An equivalent viscous damping ratio can then be found, according to Equation (3.24), which connects the Q-factor and the equivalent damping ratio, namely:

$$\zeta_{eq} = \frac{1}{2\beta}\sum_i Q_i^{-1} \tag{3.45}$$

At resonance (when the frequency ratio $\beta = 1$), the equivalent damping ratio is:

$$\zeta_{eq,r} = \frac{1}{2}\sum_i Q_i^{-1} \tag{3.46}$$

3.2.3.2 Free-Response *Q*-Factor

A damped vibratory system can also be characterized in terms of energy efficiency by formulating a Q-factor corresponding to its free response. Unlike the customary approach to the Q-factor where a harmonic force is applied to the mechanical system, the free-response Q-factor is defined based on the initial conditions of free vibrations. In the case in which an initial velocity applies to a single DOF underdamped system (the initial displacement being assumed zero), the free response of the system, according to Equation (3.5), is:

$$x(t) = \frac{\dot{x}(0)}{\omega_d} e^{-\zeta\omega_r t} \sin\left(\omega_d t\right) \tag{3.47}$$

The damping energy lost during one oscillation cycle is of the form:

$$U_d = \int F_d dx = c\int \dot{x} dx \tag{3.48}$$

After taking the time derivative of $x(t)$ from Equation (3.47), by also considering the relationship between the damping coefficient c and the damping ratio ζ (Equation (3.3)), the damping energy of Equation (3.48) can be expressed as:

$$U_d = \frac{1}{2}\left(1 - e^{-\frac{4\pi\zeta}{\sqrt{1-\zeta^2}}}\right) m\dot{x}(0)^2 \tag{3.49}$$

As Equation (3.49) suggests, the damping energy is constant for specified system parameters and initial conditions, and is not cycle-dependent (as probably expected).

The elastic energy that is stored during one oscillation cycle (when considering there are no losses) is:

$$U_d = \frac{1}{2} m\dot{x}(0)^2 \tag{3.50}$$

By using its definition of Equation (3.20), the free-response damping factor is:

$$Q = \frac{2\pi}{1 - e^{-\frac{4\pi\zeta}{\sqrt{1-\zeta^2}}}} \tag{3.51}$$

Equation (3.51) gives the *Q*-factor of a freely vibrating system as a function of the damping ratio, and this relationship is plotted in Figure 3.6.

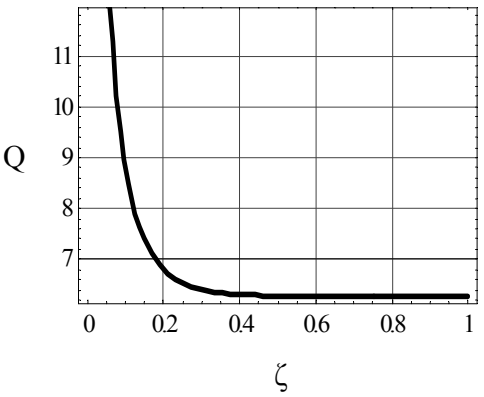

Figure 3.6 Quality factor as a function of damping ratio (underdamped case) in a free response

It can simply be shown that:

$$\begin{cases} \lim\limits_{\varsigma \to 0} Q = \infty \\ \lim\limits_{\varsigma \to 1} Q = 2\pi \end{cases} \tag{3.52}$$

While the upper limit value is expected (the *Q*-factor would go to infinity when there are no energy losses, according to Equation (3.20)), the lower limit (2π) corresponding to the critically damped case shows that the entire original kinetic energy of the system is converted to damping energy (the two energies are equal, if the factor 2π is ignored).

Example 3.5

Compare the free-response Q-factor of Equation (3.51) to the resonant Q-factor corresponding to the forced response (Equation (3.25)).

Solution:

The two Q-factors can be compared by considering their ratio, which is:

$$r_Q = \frac{4\pi\zeta}{1 - e^{-\frac{4\pi\zeta}{\sqrt{1-\zeta^2}}}} \tag{3.53}$$

This ratio function is plotted in Figure 3.7.

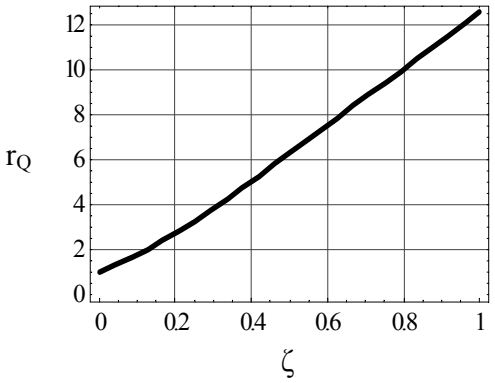

Figure 3.7 Quality factor ratio (free versus forced response) as a function of damping ratio for underdamped vibrations

It can also be shown that:

$$\begin{cases} \lim\limits_{\varsigma \to 0} r_Q = 1 \\ \lim\limits_{\varsigma \to 1} r_Q = 4\pi \end{cases} \tag{3.54}$$

Equation (3.54) indicates the two Q-factors are only equal in the absence of any viscous damping ($\zeta = 0$). In the opposite case (critically damped system, $\zeta = 1$), the Q-factor of the free response is 4π times larger than the classical, forced-response Q-factor.

As shown in subsequent sections of this chapter, an equivalent damping ratio can be formulated that incorporates all the damping sources, and therefore

an equivalent (overall) Q-factor is obtained. Equation (3.51) can be used to express the damping ratio that corresponds to a given Q-factor, namely:

$$\zeta = \frac{\ln\left(1-\frac{2\pi}{Q}\right)}{\sqrt{16\pi^2+\left[\ln\left(1-\frac{2\pi}{Q}\right)\right]^2}} \tag{3.55}$$

Example 3.6

Express the Q-factor corresponding to the free response of a single DOF mass-dashpot system when the initial conditions consist of non-zero displacement x (0). The initial velocity is assumed zero.

Solution:

When an initial displacement is applied to a mass-dashpot system, the response to this initial condition is, according to the general solution of Equation (3.5):

$$x(t) = \left[\frac{\zeta}{1-\zeta^2}\sin\left(\omega_d t\right)+\cos\left(\omega_d t\right)\right]x(0)e^{-\zeta\omega_r t} \tag{3.56}$$

The velocity function can therefore be determined, together with the damping energy lost during one vibration cycle, as shown for the case with non-zero initial velocity. By taking into account that the elastically stored energy is:

$$U_s = \frac{1}{2}kx(0)^2 \tag{3.57}$$

the Q-factor can be expressed as:

$$Q = \frac{\pi\left(1-\zeta^2\right)\left(1+\coth\frac{2\pi\zeta}{\sqrt{1-\zeta^2}}\right)}{1+\left(2\sqrt{1-\zeta^2}-1\right)\zeta^2-\zeta^4} \tag{3.58}$$

Figure 3.8 plots the relative error between the Q-factor of Equation (3.58) and the one of Equation (3.51) for damping ratios not exceeding 0.1—which is a realistic upper limit for underdamped MEMS.

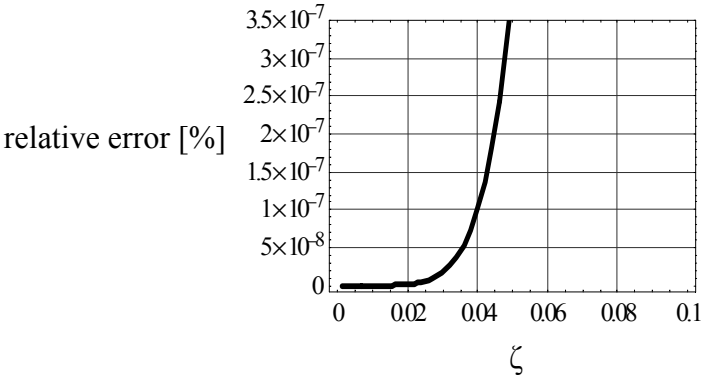

Figure 3.8 Relative errors between free-response quality factors: velocity versus displacement initial conditions

As the figure shows, the two models yield results that are in excellent agreement for the feasible domain of the damping ratio.

3.3 STRUCTURAL DAMPING

It has been shown that materials contribute to energy losses in driven systems, particularly in harmonically driven ones. In metallic materials, for instance, the energy dissipated per cycle is independent of frequency for a wide range (Thomson [1]), and is proportional to the square of the response amplitude, namely:

$$U_d = \alpha X^2 \tag{3.59}$$

Converting different forms of damping into viscous damping is advantageous from a computational standpoint because of the velocity dependency of the viscous damping. The energy loss through equivalent viscous damping during one oscillation cycle (period) is:

$$U_{d,eq} = \pi c_{eq} \omega X^2 \tag{3.60}$$

Equations (3.59) and (3.60) yield:

$$c_{eq} = \frac{\alpha}{\pi \omega} \tag{3.61}$$

The motion equation for a structurally damped system is therefore:

$$m\ddot{x} + \frac{\alpha}{\pi \omega}\dot{x} + kx = F\cos(\omega t) \tag{3.62}$$

If complex form is used again and when the following relationship is considered:

$$\dot{x} = j\omega x \tag{3.63}$$

Equation (3.62) can be rewritten as:

$$m\ddot{x} + \left(k + j\frac{\alpha}{\pi} \right) x = Fe^{j\omega t} \tag{3.64}$$

By using the notation (Thomson [1]):

$$\alpha = \pi k \gamma \tag{3.65}$$

Equation (3.62) becomes:

$$m\ddot{x} + k\left(1 + j\gamma\right) x = Fe^{j\omega t} \tag{3.66}$$

The quantity $k(1 + j\gamma)$ is called *complex stiffness* and the factor γ is the *structural damping factor*. When an exponential-form particular solution is sought for Equation (3.66), the real amplitude becomes:

$$X = \frac{F}{\sqrt{\left(k - m\omega^2\right)^2 + \gamma^2 k^2}} \tag{3.67}$$

At resonance, Equation (3.67) transforms into:

$$X_r = \frac{F}{\gamma k} \tag{3.68}$$

For viscous damping, the resonant amplitude is:

$$X_r = \frac{F}{c\omega_r} = \frac{F}{2k\varsigma} \tag{3.69}$$

Comparison of Equations (3.68) and (3.69) indicates that:

$$\gamma = 2\zeta \tag{3.70}$$

for equal resonant amplitudes. The output-input amplitude ratio (*transfer function*, as it will be shown with more detail in Chapter 4) is:

$$G(j\omega) = \frac{X}{F} = \frac{1}{k - m\omega^2 + j\gamma k} \tag{3.71}$$

whereas the *frequency response function* (also treated in Chapter 4) is:

$$H(j\omega) = \frac{kX}{F} = \frac{1}{1 - \beta^2 + j\gamma} = \frac{1 - \beta^2}{\left(1 + \beta^2\right)^2 + \gamma^2} - j\frac{\gamma}{\left(1 + \beta^2\right)^2 + \gamma^2} \tag{3.72}$$

Example 3.7

The Q-factor is determined experimentally at resonance for a metal microcantilever whose length l, cross-sectional width w, and thickness t are known. Determine the structural loss coefficient α by assuming the experimental test is conducted in vacuum (such that friction losses can be neglected), at low temperature (to discard thermal damping effects), and when support losses are disregarded.

Solution:

By taking into account Equations (3.25) and (3.70), the structural damping factor γ is expressed as:

$$\gamma = \frac{1}{Q_r} \tag{3.73}$$

which can be transformed by way of Equation (3.65) into:

$$\alpha = \frac{\pi k}{Q_r} \tag{3.74}$$

As known from elementary beam theory, the lumped-parameter stiffness of the cantilever at its free end is:

$$k = \frac{Ewt^3}{4l^3} \tag{3.75}$$

Consequently, the structural loss coefficient becomes:

$$\alpha = \frac{\pi Ewt^3}{4l^3 Q_r} \tag{3.76}$$

Equation (3.76) emphasizes that the loss coefficient is inversely proportional to the resonant Q-factor. It can also be seen that long (l large) and thin (w and t small) microcantilevers produce less structural damping.

3.4 SQUEEZE-FILM DAMPING

In squeeze-film damping, a MEMS plate-like member moves against a fixed surface and the gas in between generates a viscous damping resistance to motion, as sketched in Figure 3.9. Two particular gas regimes will be analyzed next together with their models, namely: the *continuum flow regime* and the *free molecular flow regime*.

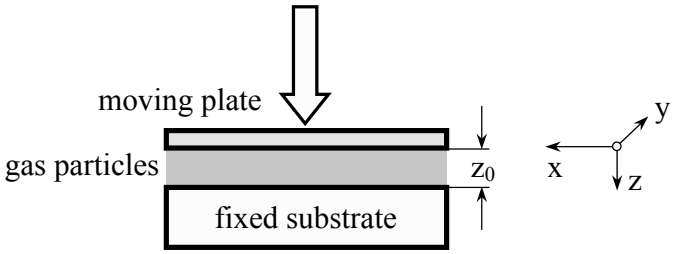

Figure 3.9 Squeeze-film damping

3.4.1 Continuum Flow Regime

In cases in which gas pressure is close to the normal (atmospheric) one and the gap is considerably larger than the free molecular path of gas molecules, the gas behaves as a continuum and approaches/results pertaining to continuum gas models are applicable.

Integration of the Poisson-type equation, which expresses the film pressure under isothermal conditions, was performed by Blech [2], for instance, who provided the following viscous damping coefficient for a rectangular plate of dimensions l and w ($l > w$):

$$c = \frac{64\sigma plw}{\pi^6 z\omega} \sum_{m,odd} \sum_{n,odd} \frac{m^2 + r^2 n^2}{m^2 n^2 \left[\left(m^2 + r^2 n^2 \right)^2 + \dfrac{\sigma^2}{\pi^4} \right]} \tag{3.77}$$

where $r = w/l$ and:

$$\sigma = \frac{12\mu_{eff} w^2}{pz^2} \omega \tag{3.78}$$

is the *dynamic squeeze-number*. In the equations above ω is the frequency of the mobile plate, p is the atmospheric pressure, z is the channel gap and μ_{eff} is the effective dynamic viscosity. The last quantity is a corrected value of a regular dynamic viscosity number, when taking into account the relationship between the gas channel dimensions and the molecular mean free path, λ,

(the distance between a molecule's two consecutive collisions). This is best expressed by the *Knudsen number*:

$$Kn = \frac{\lambda}{z} \tag{3.79}$$

Veijola et al. [3], for instance, suggest the effective dynamic viscosity:

$$\mu_{eff} = \frac{\mu}{1 + 9.638 Kn^{1.159}} \tag{3.80}$$

which is an accurate prediction for the range $0 < Kn < 880$.

The dynamic squeeze number σ, as indicated by Blech [2], is also an indicator of the necessity of considering the spring effect of gas trapped between the two plates at values of $\sigma > 3$. In such situations, the equivalent spring constant of the gas was found to be:

$$k = \frac{64\sigma^2 plw}{\pi^8 z} \sum_{m,odd} \sum_{n,odd} \frac{m^2 + r^2 n^2}{m^2 n^2 \left[\left(m^2 + r^2 n^2 \right)^2 + \frac{\sigma^2}{\pi^4} \right]} \tag{3.81}$$

Example 3.8

Compare the viscous damping coefficient of Equation (3.77) when the first four terms of the double series are retained with the viscous damping coefficient provided by Zhang et al. [4], namely:

$$c = \frac{96}{\pi^4} \frac{l^3 w^3}{l^2 + w^2} \frac{\mu}{z^3} \tag{3.82}$$

Consider that air pressure is p = 100,000 N/m^2, dynamic viscosity is $\mu = 1.85 \times 10^{-5}$ N-s/m^2, and use the first level of approximation.

Solution:

For $m = n = 3$, Equation (3.77) gives a damping coefficient denoted by c_{33}. When the plate's geometry is of interest, one can select an operating frequency and a gap distance, for instance, f = 500,000 Hz and z = 10 μm. By also using the other numerical values of this example, the plot of Figure 3.10 is obtained, which shows the relative errors between c_{33} and c, calculated as:

$$e = \frac{c - c_{33}}{c_{33}} \tag{3.83}$$

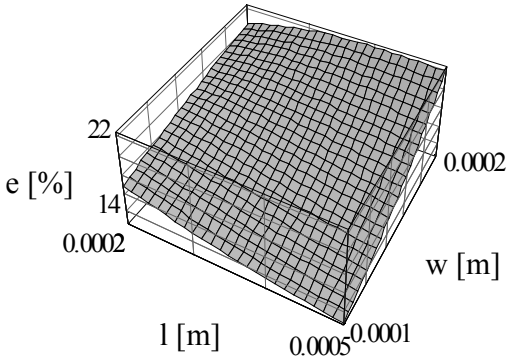

Figure 3.10 Relative errors in damping coefficients in terms of plate geometry in squeeze-film damping

For l = 200 μm and w = 50 μm, the plot of Figure 3.11 is obtained, which indicates the influence of vibration frequency and gap dimension on the same damping coefficient ratio.

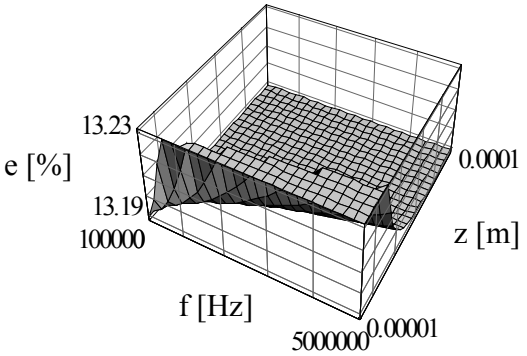

Figure 3.11 Relative error in damping coefficients in terms of vibration frequency and gap dimension in squeeze-film damping

Example 3.9

Analyze the precision of calculating the squeeze-film damping coefficient of Equation (3.77) as a function of the number of n and m terms in the corresponding infinite series.

Solution:

The squeeze number of Equation (3.77) is expressed as a series expansion in m and n. The double sum that defines it is expressed next by taking several levels of approximation, namely:

$$S_{1,1} = \frac{1+r^2}{\left(1+r^2\right)^2 + \dfrac{\sigma^2}{\pi^4}} \tag{3.84}$$

$$S_{3,3} = \sum_{m=1,\, m-odd}^{3} \sum_{n=1,\, n-odd}^{3} \frac{m^2 + r^2 n^2}{m^2 n^2 \left(m^2 + r^2 n^2\right)^2 + \dfrac{\sigma^2}{\pi^4}} \tag{3.85}$$

$$S_{5,5} = \sum_{m=1,\, m-odd}^{5} \sum_{n=1,\, n-odd}^{5} \frac{m^2 + r^2 n^2}{m^2 n^2 \left(m^2 + r^2 n^2\right)^2 + \dfrac{\sigma^2}{\pi^4}} \tag{3.86}$$

Equations (3.84), (3.85), and (3.86) are used to form the following relative error numbers:

$$\begin{cases} e_{11-33} = \dfrac{\left|S_{11} - S_{33}\right|}{S_{11}} \\ e_{11-55} = \dfrac{\left|S_{11} - S_{55}\right|}{S_{11}} \\ e_{33-55} = \dfrac{\left|S_{33} - S_{55}\right|}{S_{33}} \end{cases} \tag{3.87}$$

For a squeeze number $\sigma = 10$, the percentage errors defined in Equation (3.87) are plotted in Figure 3.12 in terms of the non-dimensional variable $r = w/l$.

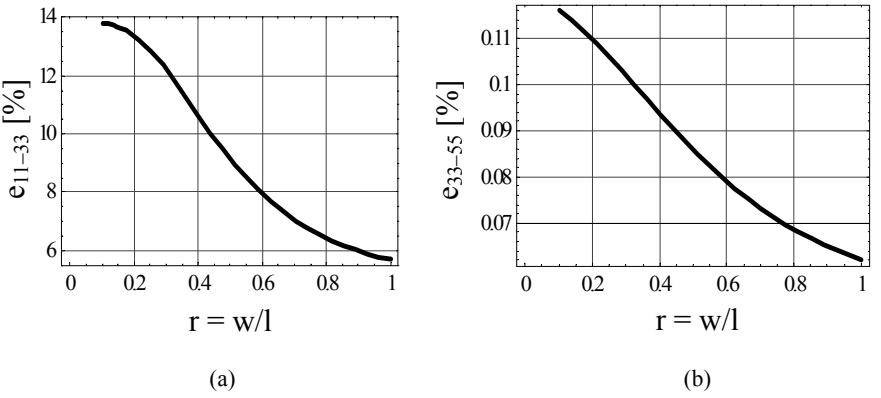

(a) (b)

Figure 3.12 Relative errors in computing the squeeze number

As Figure 3.12 shows, the relative errors decrease sharply from the third level of approximation (when six terms are retained from the series; Equation (3.86)), which is compared to the second level of approximation (when four terms are retained from the series, as shown in Equation (3.85)). The relative error e_{11-55} of Equation (3.87) is very similar to the error e_{33-55} and was not plotted here. It is therefore safe, in terms of accuracy, to truncate the series expansion involved in calculating the viscous damping coefficient corresponding to the squeeze film phenomenon at $m = n = 3$.

Example 3.10

Analyze the squeeze number variation with respect to the width of a microplate that moves against a fixed plate and the spacing between the two plates in the case of air. Known are the following amounts: molecular free mean path $\lambda = 85$ μm, dynamic viscosity coefficient $\mu = 1.85 \times 10^{-5}$ N-s/m, pressure $p = 101{,}325$ N/m^2, frequency $f = 100$ MHz.

Solution:

With the numerical values given in this problem, and by taking into account that $\omega = 2\pi f$, the squeeze number becomes:

$$\sigma = \frac{1.375}{1 + 6.15e^{-8} z^{-1.159}} \left(\frac{w}{z} \right)^2 \tag{3.88}$$

Figure 3.13 shows the variation of the squeeze number in terms of the plate width and the spacing. Figure 3.14 gives the squeeze number dependency of the gap for a fixed width $w = 800$ μm.

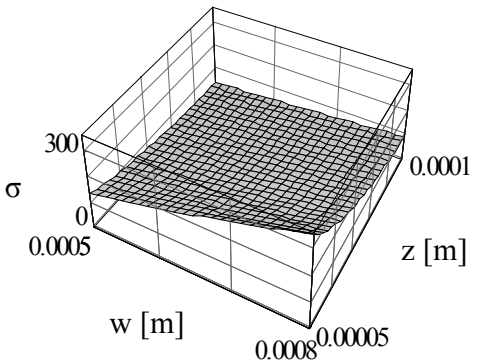

Figure 3.13 Squeeze number as a function of plate width w and gap z

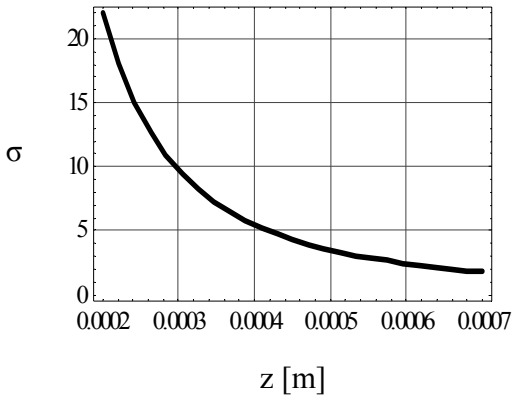

Figure 3.14 Squeeze number as a function of gap z

Solving the equation $\sigma = 3$, where σ is given in Equation (3.78) results in $z =$ 541.5 μm. Figures 3.13 and 3.14 indicate that σ decreases with the gap increasing and therefore, according to Blech's prescription, for gaps larger than 541.5 μm, air escapes the gap and the additional spring behavior is not manifested.

Example 3.11

Examine the influence of gas entrapping ($\sigma = 10$) in a paddle microbridge (Figure 3.15) on its bending-related resonant frequency. Assume the out-of-the-plane motion of the paddle segment is always parallel to the substrate.

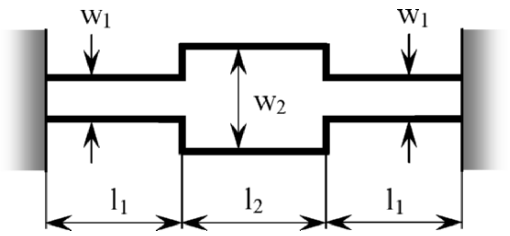

Figure 3.15 Top view of paddle bridge with dimensions

Solution:

When only considering the elasticity of the end segments of a paddle microbridge (as the one shown in Figure 3.15), the stiffness corresponding to out-of-the-plane bending (about the y-axis) is:

$$k_{b,y} = 2\frac{12EI_y}{l_1^3} = 2\frac{Ew_1t^3}{l_1^3} \tag{3.89}$$

In the case air is entrapped between the out-of-the-plane vibrating middle plate and substrate, the corresponding spring effect is expressed by the stiffness given in Equation (3.81) and the total stiffness is the one of a spring parallel connection, namely:

$$k_{b,y}^{tot} = 2\frac{Ew_1t^3}{l_1^3} + \frac{64\sigma^2 pl_2w_2}{\pi^8 z}\sum_{m,odd}\sum_{n,odd}\frac{m^2+r^2n^2}{m^2n^2\left[\left(m^2+r^2n^2\right)^2+\dfrac{\sigma^2}{\pi^4}\right]} \tag{3.90}$$

The mass of the microbridge is considered to be provided by the middle segment, which, according to Figure 3.15, is:

$$m = \rho w_2 l_2 t \tag{3.91}$$

When taking a one-term series approximation in Equation (3.90) ($m = n = 1$), the following resonant frequency percentage error can be formulated:

$$e_\omega = \frac{\omega_{b,y}^{total} - \omega_{b,y}}{\omega_{b,y}} = \frac{\sqrt{k_{b,y}^{total}} - \sqrt{k_{b,y}}}{\sqrt{k_{b,y}}} \tag{3.92}$$

Equation (3.92) has been used to draw Figures 3.16 and 3.17. Figure 3.16 is plotted for $l_2 = 200$ μm and $w_2 = 100$ μm, whereas Figure 3.17 is plotted for $l_2 = 200$ μm and $w_1 = 50$ μm.

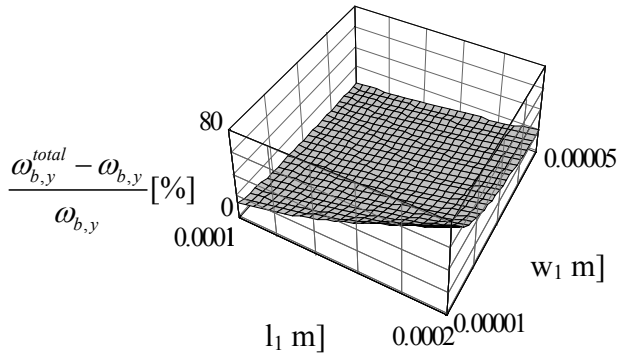

Figure 3.16 Relative errors in bending resonant frequency of a paddle microcantilever ($l_2 = 200$ μm, $w_2 = 100$ μm)

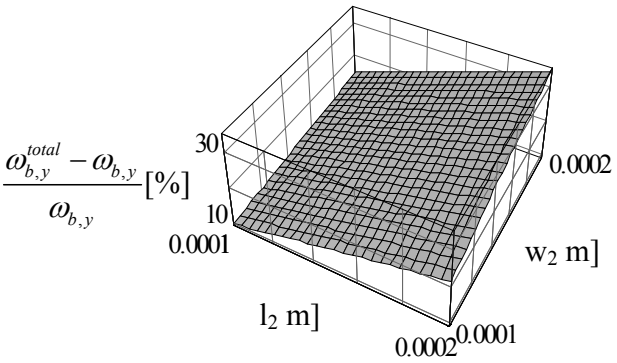

Figure 3.17 Relative errors in bending resonant frequency of a paddle microcantilever (l_1 = 200 μm, w_1 = 50 μm)

As Figure 3.16 indicates, the relative differences between the out-of-the-plane bending resonant frequency when air elasticity is taken into account and the one in which air elasticity is not considered, increase with the length of the mid-segment increasing and the width decreasing up to a maximum of 80% for the selected parameter ranges. The effects of length and width of the root segment (the flexible ones) on the same resonant frequency differences are shown in Figure 3.17, which indicates that differences do increase with both length and width, increasing up to a relative maximum of 25% for the parameters analyzed in the figure.

3.4.2 Free Molecular Flow Regime

The squeeze-film damping models presented thus far are accurate for situations in which the gas behaves as a continuum, and this condition is satisfied when the pressure is not very low, because in such cases the mean free molecular path of gas molecules is less than the plate gap (which amounts to the Knudsen number of Equation (3.69) being less than one, $Kn < 1$). The mean free molecular path is defined by the following equation:

$$\lambda = \frac{RT}{\sqrt{2}\pi d^2 N_A p} \tag{3.93}$$

where R is the universal gas constant, T is the absolute temperature, d is the gas molecule diameter, N_A is Avogadro's number (which gives the number of molecules in a mole of substance), and p is the pressure. For air, R = 8.314 J/mol-K, $N_A = 6.022 \times 10^{23}$, and the molecular diameter is $d = 3 \times 10^{-10}$ m. In case of a normal temperature of 300°K, the mean free molecular path of Equation (3.93) becomes:

$$\lambda = \frac{0.01}{p} \tag{3.94}$$

Under normal pressure conditions, such as $p = 100{,}000$ N/m^2, the mean free molecular path is $\lambda = 0.1$ μm, whereas for small pressures (almost vacuum), such as $p = 1$ N/m^2, the mean free molecular path is $\lambda = 1$ cm. Regular gaps in MEMS are of the order of micrometers, and therefore, for low (vacuum) pressures, the molecular mean free path is much smaller than the gap in a squeeze-film situation. Consequently, the continuum laws are no longer applicable and models pertaining to the free molecular domain are in place. By using notions of the momentum transfer, the Christian model [5], gives the following estimate of the Q-factor due to air damping at low pressures:

$$Q = \left(\frac{\pi}{2}\right)^{\frac{3}{2}} \frac{\rho t \omega}{p} \sqrt{\frac{RT}{M_m}} \tag{3.95}$$

where ρ is the gas mass density, t is the plate thickness, p is the pressure, and M_m is the molar weight of gas. This model assumed an infinitely large volume and considered the Maxwell-Boltzmann distribution of gas velocity. The results of Christian's model (which was derived for macroscale applications) indicated Q-factors larger than experimental measurements indicated. Kadar et al. [6] used a variant of the Maxwell-Boltzmann distribution, namely the Maxwell stream distribution, and proposed the following Q-factor:

$$Q = \frac{1}{\pi}\left(\frac{\pi}{2}\right)^{\frac{3}{2}} \frac{\rho t \omega}{p} \sqrt{\frac{RT}{M_m}} = \sqrt{\frac{\pi}{8}} \frac{\rho t \omega}{p} \sqrt{\frac{RT}{M_m}} \tag{3.96}$$

which is essentially π times smaller than Christian's model prediction.

Bao et al. [7] propose a similar Q-factor model that accounts for the plate dimensions and gap, namely:

$$Q = (2\pi)^{\frac{3}{2}} \frac{\rho t \omega}{p} \frac{z}{2(l+w)} \sqrt{\frac{RT}{M_m}} \tag{3.97}$$

where z is the gap and l and w are the dimensions of a rectangular plate. This model also considers the energy transfer from the oscillating plate to the gas and the reflection wall effects.

Example 3.12

A plate with $l = 180$ μm, $w = 40$ μm, and $t = 1$ μm is suspended by two single-wall carbon nanotubes (SWCNTs) 1.4 in diameter and oscillates out-of-the-plane against the substrate in air at normal temperature $T = 300$°K and at a frequency of $f = 1$ MHz. Calculate the length of the SWCNT beams that will render the continuum-model and molecular-model Q-factors equal. Consider the following numerical properties: free gap $z = 10$ μm, pressure $p = 1000$ N/m^2.

Solution:

For air, the molecular weight is $M_m = 0.029$ kg/mol and the molecular diameter is $d = 3 \times 10^{-10}$ m; the gas constant is $R = 83145$ J/mol-K and the density at sea level and normal temperature is 1.2 kg/m^3. With the numerical data of the example and with the aid of Equation (3.94), it is found that the molecular free path is $\lambda = 10$ μm, which is equal to the equilibrium gap, and therefore both the continuum and molecular models are likely to be valid. The continuum-model Q-factor is obtained from the corresponding damping coefficient as:

$$Q_c = \frac{k}{c\omega} \tag{3.98}$$

It can be seen that this Q-factor depends on the spring stiffness, whereas the molecular-model Q-factor does not depend on any stiffness. Anyway, in order for the two models' Q-factors to be equal, the stiffness needs to have a specified value. By calculating the two models' Q-factors, an equation in k results, which gives $k = 17.27$ N/m. At the same time, it is known from mechanics of materials that the stiffness of a clamped-guided beam is:

$$k = \frac{3\pi d^4 E}{16 l_b^3} \tag{3.99}$$

where E is the elastic modulus of the beam. An average value of $E = 10^{12}$ N/m^2 will be considered, and l_b is the unknown beam length. The total stiffness is twice the one given in Equation (3.99) because there are two beams supporting the plate, and therefore by equating that stiffness to the number found above, the resulting beam length is $l_b = 11.18$ nm.

Bao's model assumed constant gas particle velocity, and, in addition, the amplitude of oscillations was considered much smaller than the gap dimension. The time interval when a molecule is located between the resonator and the wall was assumed to be much smaller than the plate oscillation period. Hutcherson and Ye [8] proposed a Q-factor model that was two times smaller

than the *Q*-factor, according to Bao's model prediction. This model allowed for variations in the gas particle velocity and was proved to be valid for situations in which the ratio of the gap to the plate length is around 1/200.

The *Q*-factor in squeeze-film damping is further affected by gas–surface interactions, of which out gassing from surfaces and gas molecule adsorption by the plates are the most important. A quantifier of these interactions is the *normal momentum accommodation coefficient* (NMAC), α_n, which ranges from 0 for no adsorption to 1 for full adsorption. Polikarpov et al. [9] proposed the following damping ratio, which took into account the gas–surface adsorption interaction:

$$\zeta = \frac{2-\alpha_n}{\rho t} p\sqrt{\frac{2m_m}{\pi kT}} \tag{3.100}$$

where ρ is the plate's material mass density, t is the plate thickness (as previously mentioned), m_m is the molecular mass of the gas, k is Boltzmann's constant, and T is the absolute temperature. By taking Equation (3.24) into account, which defines the relationship between the damping ratio and the *Q*-factor, the latter can be expressed by also considering that:

$$\frac{m_m}{k} = \frac{M_m}{R} \tag{3.101}$$

as:

$$Q = \left(\frac{\pi}{2}\right)^{\frac{3}{2}} \frac{2}{2-\alpha_n} \frac{\rho t f}{p} \sqrt{\frac{RT}{M_m}} \tag{3.102}$$

Equation (3.102) also considered the relationship between the angular frequency ω and the normal one f, namely: $\omega = 2\pi f$.

3.4.3 Squeeze-Film Damping for Rotary-Motion Plates

Equivalent viscous damping coefficients expressed so far that involved squeeze-film damping referred to translation and therefore were related to linear-motion damping forces. In the case sketched in Figure 3.18, a plate rotates about a fixed pivot point and the gas is squeezed between the moving plate and the fixed substrate producing a damping torque, which opposes the motive angular velocity ω.

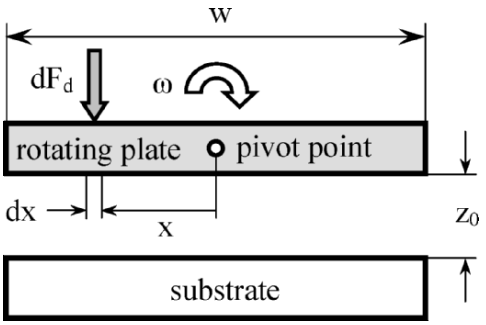

Figure 3.18 Squeeze-film damping and rotary plate

This topic has usually been approached by linearizing the Reynolds equation that expressed the variable pressure about the *x*-direction under the assumption that the angular motions of the plate are small compared to the static gap z_0. The linearized equation is subsequently solved, and its solution is used to determine the total resistive damping torque (Darling et al. [10], Dotzel et al. [11], Pan et al. [12] and Bao et al. [13], to cite just a few of the work dedicated to this topic). Veijola et al. [14] presented a simple model that yielded the damping coefficient pertaining to a plate rotating at an angular velocity ω, which is connected to the corresponding torque as:

$$M_d = c_r \omega \tag{3.103}$$

The model starts by considering the linearized, temperature-independent Reynolds equation in one dimension (the *x*-direction):

$$\frac{z_0^2}{12\mu_{eff}} \times \frac{d^2 p(x)}{dx^2} = \frac{\omega x}{z_0} \tag{3.104}$$

where the linear velocity of the plate at a distance *x* measured from the central pivot point is simply $\omega \times x$, and p_0 is the ambient (constant) pressure. The solution to Equation (3.104) is a third-order polynomial and its two integration constants are determined by applying the trivial boundary conditions:

$$p\left(w/2\right) = p\left(-w/2\right) = 0 \tag{3.105}$$

The pressure is therefore:

$$p(x) = c_1 \left(4\frac{x^3}{w^3} - \frac{x}{w} \right) \tag{3.106}$$

where:

$$c_1 = \frac{\mu_{eff}\omega w^3}{2z_0^3} \tag{3.107}$$

The elementary damping force acting on an elementary surface area dA = dxdy and opposing the plate rotation can be expressed as:

$$dF_d = p(x)dxdy \tag{3.108}$$

and this force produces an elementary damping torque:

$$dM_d = xdF_d = xp(x)dxdy \tag{3.109}$$

The total damping torque is found by integrating Equation (3.109) over the whole plate area, namely:

$$M_d = \int_A dM_d = \int_{-l/2}^{l/2}\left[\int_{-w/2}^{w/2} xp(x)dx\right]dy \tag{3.110}$$

After integration and consideration of Equation (3.103), which gives the relationship between damping torque and angular velocity, the torsional damping coefficient is expressed as:

$$c_r = \frac{\mu_{eff} w^5 l}{60 z_0^3} \tag{3.111}$$

Example 3.13

A plate is suspended at its ends by two serpentine springs that are clamped at their opposite ends to the substrate, as sketched in Figure 3.19. Compare the squeeze-film damping that is generated when the plate moves out-of-the plane parallel to the substrate to the damping corresponding to the small-angle rotation of the plate about the x-axis.

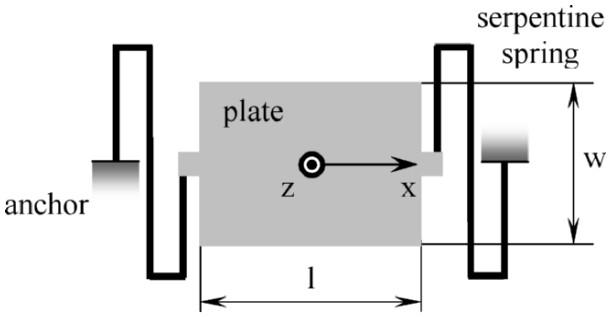

Figure 3.19 Plate with two end serpentine springs

Solution:

The damping comparison is carried out by means of the resonant Q-factors, which, according to the definition of Equation (3.25), depend on inertia, damping, and stiffness. For the translatory motion about the z-axis, the Q-factor is:

$$Q_z = \frac{\sqrt{MK_z}}{c_z} \tag{3.112}$$

where M is the mass of the plate, c_z (Equation (3.82)) is the damping coefficient of the z-axis translation, and K_z is the stiffness of the spiral springs corresponding to the same motion. Similarly, the Q-factor defining damping due to squeeze-film effects accompanying the resonant rotary vibrations of the plate can be expressed as:

$$Q_r = \frac{\sqrt{K_r J_x}}{c_r} \tag{3.113}$$

where J_x is the plate mechanical moment of inertia about the x-axis, c_r (Equation (3.111)) is the damping coefficient of this motion and K_r is the torsional stiffness of the two serpentine springs. The plate's moment of inertia depends on mass as:

$$J_x = \frac{M}{12}\left(w^2 + t_p^2\right) \tag{3.114}$$

where t_p is the plate thickness.

The stiffness of a serpentine spring expressing translatory motion about the z-axis in Figure 3.19 was given by Lobontiu and Garcia [15], and because there are two springs in parallel in this application, the corresponding stiffness is twice the one of an original spring, namely:

$$K_z = \frac{3EGI_y I_t}{3EI_y l_1 l_2 (l_1 + 3l_2) + 2GI_t (l_1^3 + 2l_2^3)} \tag{3.115}$$

Similarly, Lobontiu and Garcia [15] derived the torsional stiffness of a spiral spring that defines rotation about the x-axis of Figure 3.19. The total torsional stiffness of this application is twice the one of an original spiral spring, namely:

$$K_r = \frac{EGI_y I_t}{EI_y l_2 + 2GI_t l_1} \tag{3.116}$$

In Equations (3.115) and (3.116), E and G are the longitudinal and shear modulii of the spring material, whereas l_1 is the length of half of a long leg defining the spiral spring and l_2 is the length of a spring short leg, as also shown in a previous example in Chapter 1. Figure 3.20 shows the cross-section of a spiral spring, which is assumed constant and identical for both the long and short legs.

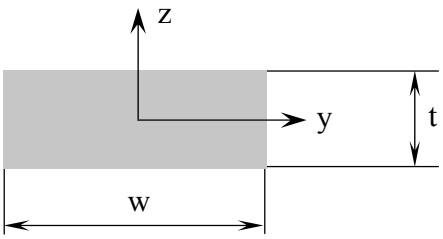

Figure 3.20 Cross-sectional dimensions of the spiral spring

Considering the cross-section is thin, the moments of inertia are related as:

$$I_t = 4I_y = \frac{wt^3}{3} \tag{3.117}$$

All the amounts that are necessary to compute the Q-factors of Equations (3.112) and (3.113) are now available. The non-dimensional variables c_1, c_2, c_w, and c_t are introduced and defined as follows: $l_1 = c_1 \times l$, $l_2 = c_2 \times l$, $w = c_w \times l$, $t_p = c_p \times l$. The plots of Figure 3.21 show the variation of the rotation-to-translation Q-factor ratio. In Figure 3.21 (a), $c_1 = 0.5$ and $c_2 = 0.1$, whereas in Figure 3.21 (b), $c_w = 0.2$ and $c_t = 0.01$.

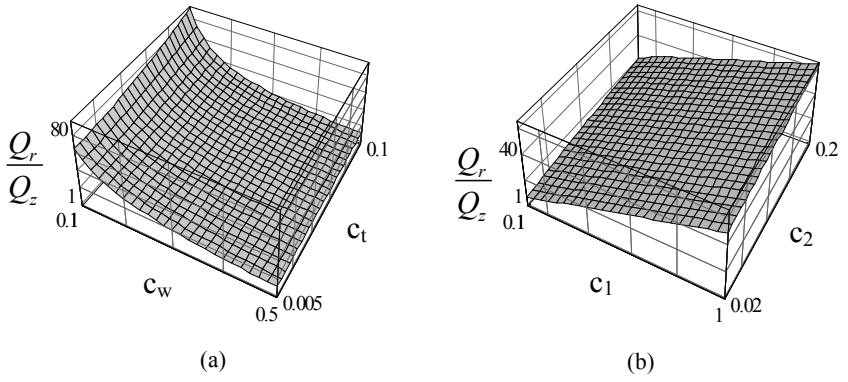

Figure 3.21 Numerical simulation for rotary-to-translatory quality factor ratio for squeeze-film damping: (a) $c_1 = 0.5$, $c_2 = 0.1$; (b) $c_w = 0.2$, $c_t = 0.01$

3.4.4 Squeeze-Film Damping: Translatory Perforated Plates

Proper operation of MEMS/NEMS under squeeze-film damping conditions is often times hampered by the relatively high damping coefficients (particularly for thick plates), which reduce the device Q-factor. An alternative to using slide-film damping instead of squeeze-film damping or to packaging the device in low-pressure cells is to perforate the plate, which allows air to flow through from the gap and therefore reduce damping. Finding the damping coefficient under the presence of a number of holes in the original plate implies modification of the original Reynolds's pressure equation so that the perforation region is taken into consideration. The damping force can be computed subsequently, and is of the form: damping coefficient times plate velocity; this procedure yields the damping coefficient. Of the many contributions to this area, Bao et al. [16, 17] proposed the approach of dividing the plate into cells with holes at centers, as shown, for instance, in Figure 3.22.

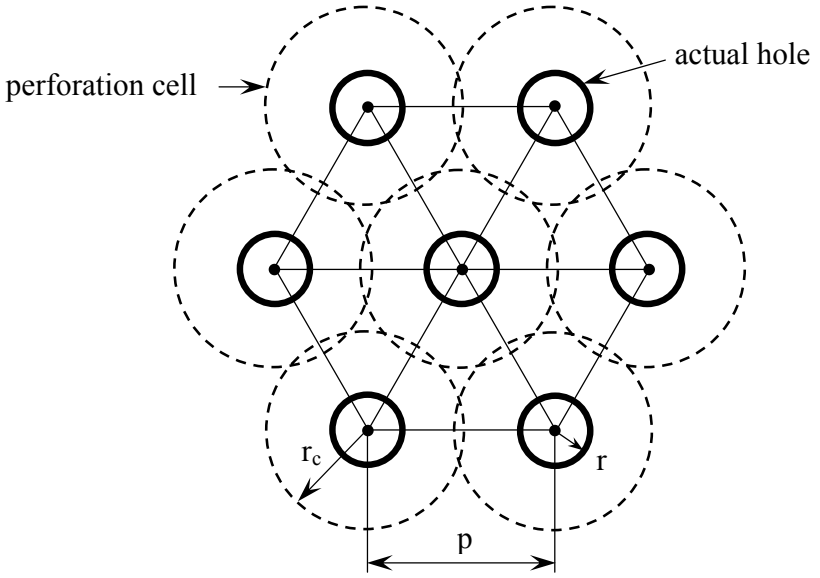

Figure 3.22 Portion of hole-plate showing actual hole and perforation cell arrangement

They assumed the pressure is a smooth function of position under the entire plate and that the fluid actually flowing through the physical hole penetrates the whole cell. Another assumption of their model is that flow through the hole (about the z-direction) is *fully developed Poiseuille flow*, which is a pressure-driven flow, and has a curvilinear symmetric profile with zero velocity at the edges and maximum velocity at the hole center. In doing so, the actual area of a rectangular plate, for instance, is transformed into an equivalent smaller area where pressure acts uniformly, as indicated in Figure 3.23.

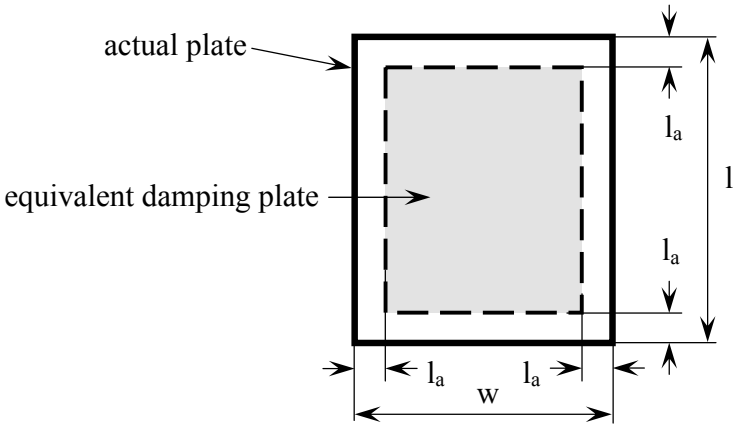

Figure 3.23 Top view of actual and equivalent damping plate

By applying this procedure, the following damping coefficient is obtained under the additional assumption that at least three holes exist across the plate in any direction:

$$c = \frac{12\mu}{z_0^3} l_a^2 \left(w - 2l_a\right)\left(l - 2l_a\right) \tag{3.118}$$

where w and l are the plate in-plane dimensions, z_0 is the original (static) gap, μ is the dynamic viscosity (which for slip and transition regimes can be substituted by μ_{eff} [Equation (3.80)], according to Veijola et al. [3]), and l_a is the *attenuation length* (Bao et al. [16, 17]), which is computed as:

$$l_a = \sqrt{\frac{2z_0^3 t_{eff}\eta(\beta)}{3\beta^2 r^2}} \tag{3.119}$$

In Equation (3.119), t_{eff} is the effective thickness of the plate, which takes into account additional flow resistance at the perforation ends (particularly when the hole radius r compares to the plate thickness t), and is calculated as:

$$t_{eff} = t + \frac{3\pi r}{8} \tag{3.120}$$

The coefficient β in Equation (3.119) is the ratio between the hole radius r and the perforation cell radius r_c, namely: $\beta = r/r_c$. In the same Equation (3.119):

$$\eta(\beta) = 1 + \frac{3r^4\left(4\beta^2 - \beta^4 - 4\ln\beta - 3\right)}{16tz_0^3} \tag{3.121}$$

The radius of the perforation cell can be computed based on Figure 3.22 by following the procedure developed by Mohite et al. [18], for instance. The holes and their perforation cells (circles) can be grouped in the hexagonal arrangement shown in the same figure. The area of the hexagon coupling the seven circles is approximately equal to the area of the center cell plus six identical cell areas, each equal to one-third the area of a full cell. Consequently, the hexagon area equals a total of three cell areas, namely:

$$6\times\left(\frac{1}{2}\times p\times\frac{\sqrt{3}}{2}p\right)=3\times\left(\pi r_c^2\right) \tag{3.122}$$

Equation (3.122) gives the radius of the cell as a function of the pitch distance p between two adjacent plate holes:

$$r_c=0.525p \tag{3.123}$$

Example 3.14

Study the influence of the pitch dimension p on the attenuation length and of the squeeze-film damping of a rectangular plate with holes in it. The plate's dimensions are l = 500 μm, w = 100 μm, t = 2 μm. The initial gap is z_0 = 10 μm and the air's dynamic viscosity is $\mu = 1.73\times10^{-5}$ N-s/m^2.

Solution:

By using the given numerical data, Equations (3.118) through (3.123) are used to express l_a and c in terms of only the pitch distance p and the hole radius r. Figure 3.24 shows the two functions plotted against p and r. Both the attenuation length and the damping coefficient increase with the pitch distance in a quasi-linear fashion, as shown in Figure 3.24, whereas the magnitude of the hole radius has a nonlinear influence, which is, however, smaller compared to the influence of the pitch distance.

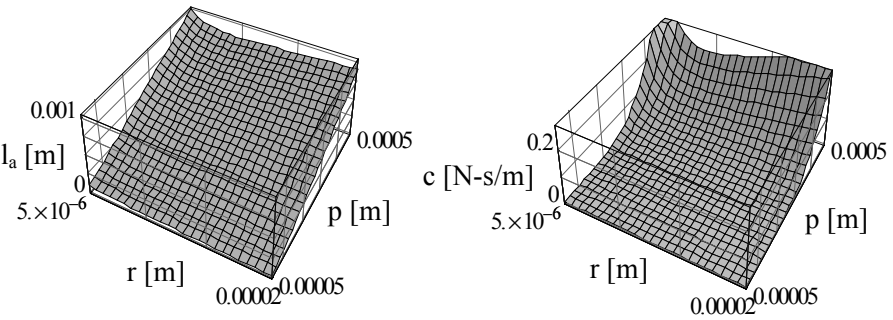

Figure 3.24 Damping characteristics for a plate with holes: (a) attenuation length; (b) damping coefficient

3.5 SLIDE-FILM DAMPING

When the motion of a plate takes place parallel to another fixed plate (such as the substrate in a MEMS device), shearing of the fluid underneath and above the moving plate will generate viscous damping resistance through the relative fluid-structure sliding. The slide-film damping is sketched in Figure 3.25.

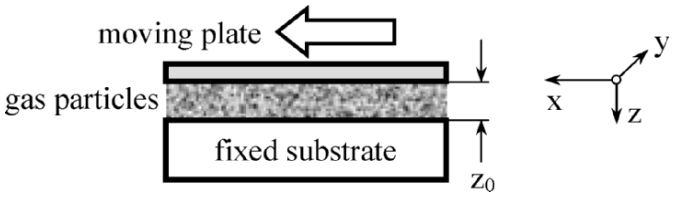

Figure 3.25 Slide-film damping

Depending on the Knudsen number, which compares the mean free molecular path to the fluid path, there are normally four different flow types, and the damping coefficients are determined by different models. For Knudsen numbers smaller than 0.001, which means the free molecular path is at least three orders of magnitudes smaller than the fluid gap, the viscous damping can be assessed by macro-scale, conventional methods pertaining to *continuum models*. Larger values of the *Kn* number indicate the mean free molecular path and gap dimension become comparable and micro/nano phenomena such as gas rarefaction and gas–surface interactions have to considered. As such, when $0.001 < Kn < 0.1$, the flow is known as *slip flow*, and slip velocity boundary conditions have to be accounted for. To determine the damping coefficients, Navier-Stokes equations are solved for both flow categories. For $0.1 < Kn < 10$, *transition flow* conditions are set up, while for $Kn > 10$ the flow is *free molecular*. These cases are discussed next.

3.5.1 Continuum Flow Regime

In the case of Knudsen numbers that are less than 0.001, the flow is governed by macro-scale laws and the viscous damping coefficient is determined as follows. The boundary conditions are considered fixed, namely:

$$\begin{cases} v_x(0) = 0 \\ v_x(z_0) = v \end{cases} \tag{3.124}$$

The shearing stresses present between two adjacent fluid layers in one-dimensional flow are expressed (e.g., see Landau and Lifschitz [19]) as:

$$\tau = \mu \frac{dv_x(z)}{dz} \tag{3.125}$$

One model that enables predicting the damping coefficient is the *Couette model*, according to which the velocity profile of the fluid between the two plates varies linearly from 0 (at the fixed plate) to the mobile plate velocity at the interface with it. The fluid above the moving plate is assumed to displace with a velocity equal to that of the plate, as sketched in Figure 3.26 below. As a direct consequence, damping is only generated by the fluid between the two plates.

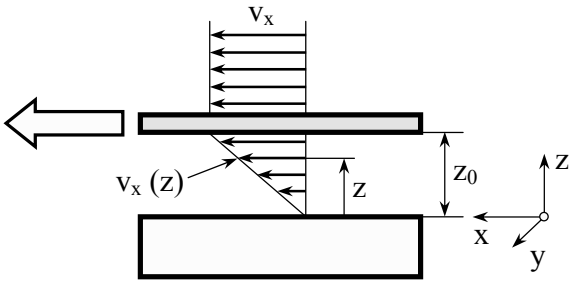

Figure 3.26 Velocities in Couette slide-film damping

For Couette-type flow, the linear velocity profile of Figure 3.26 is expressed as:

$$v_x(z) = \frac{z}{z_0} v_x \tag{3.126}$$

By combining Equations (3.125) and (3.126), the shearing stress becomes:

$$\tau = \mu \frac{v_x}{z_0} \tag{3.127}$$

which indicates the stress is constant over the two plates gap. The damping force produced at the plate–fluid interface can be calculated by multiplying the shear stress to the mobile plate area, namely:

$$F_d = \tau A = \frac{\mu A}{z_0} v_x \tag{3.128}$$

A linear damping force is the product of a damping coefficient to the velocity, and therefore Equation (3.128) yields the following viscous damping coefficient owing to Couette-type slide-film effects:

$$c_C = \frac{\mu A}{z_0} \tag{3.129}$$

The corresponding Q-factor of Equation (3.24) can be calculated by means of c_C from Equation (3.129) as:

$$Q_C = \frac{kz_0}{\mu A\omega} \tag{3.130}$$

where k is the spring stiffness associated with the mobile plate (which is elastically supported over the substrate) and ω is the frequency of the sinusoidal force that drives the mobile plate. At resonance, when the driving force frequency equals the plate-spring resonant frequency, the Couette-type Q-factor becomes:

$$Q_{C,r} = \frac{z_0}{\mu A}\sqrt{km} \tag{3.131}$$

where m is usually the mass of the moving plate. Equation (3.130) indicates that the Q-factor increases by reducing the dynamic viscosity of the gas, as well as the plate area, and by increasing the gap, together with the mass and stiffness of the plate-spring system.

Example 3.15

A plate microresonator, as the one sketched in Figure 3.27, is driven at resonance by a comb-drive actuator. The plate is elastically supported by two spiral springs. Design a plate-spring system that will have a specified Q-factor at resonance for given air viscosity and plate gap. Assume also that the plate area is known and that the plate-to-spring thickness ratio and the spring's leg length ratio (the spring is shown in Figure 3.28) are specified as well.

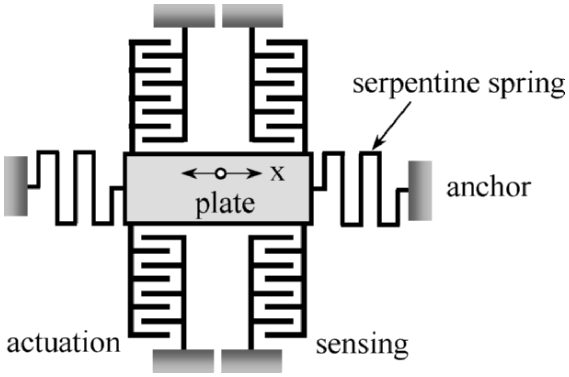

Figure 3.27 Electrostatically actuated and sensed microplate resonator with spiral springs (top view)

Solution:

Equation (3.131) can be rewritten as:

$$Q_{C,r} = \frac{z_0}{\mu}\sqrt{\frac{\rho k t}{A}} \tag{3.132}$$

where ρ is the plate's mass density and t is its thickness. The total stiffness of this microresonator is twice the stiffness of a single spring because there are two springs here acting in parallel. The stiffness of a spiral spring can be found as the inverse of the compliance given by Lobontiu and Garcia [15] as:

$$k = \frac{3EI_z}{2l_1^2\left(2l_1 + 3l_2\right)} \tag{3.133}$$

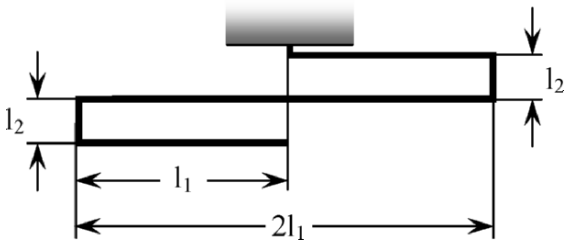

Figure 3.28 Geometry of spiral spring unit

The geometry of a spiral spring unit is shown in Figure 3.28, but each of the springs shown in Figure 2.27 is formed of two serially connected spiral spring units, and the total stiffness is therefore the equivalent stiffness of the spring arrangement shown in Figure 3.29.

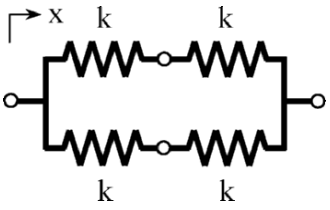

Figure 3.29 Spring arrangement for the microresonator of Figure 3.28

By serially combining two identical spiral units to form one full spiral spring, the resulting stiffness becomes half the one of Equation (3.133). By further combining the two resulting springs in parallel, the final equivalent stiffness

is twice the one of a serial chain, and therefore equal to the one of the original spring unit of Equation (3.133). By considering the spring cross-section is square with a thickness t_s, the Q-factor of Equation (3.132) becomes:

$$Q_{C,r} = c\frac{t^{5/2}}{l_2^{3/2}} \tag{3.134}$$

where:

$$c = \frac{z_0 c_t^2}{2\mu c_l}\sqrt{\frac{\rho E}{2A\left(3+2c_l\right)}} \tag{3.135}$$

has the dimension of length to the – (2/5) power and with: $l_1 = c_l l_2$, and $t_s = c_t t$. Equation (3.134) suggests that the Q-factor can be improved by increasing the plate and spring thickness and by shortening the legs of the spiral spring. By selecting one parameter, for instance l_2, the other unknown can be computed as:

$$t = \left(\frac{Q_{C,r}}{c}\right)^{2/5} l_2^{3/5} \tag{3.136}$$

3.5.2 Slip Flow Regime

Slip flow regimes are set up for Knudsen numbers $0.001 < Kn < 0.1$, when the mean free molecular path-to-gap ratio increases and when the gas velocity is not zero at the gas-fixed surface interface due to some gas molecular motion. The flow velocity is still linear (the Couette flow). For relatively slow motion of the plate (when gas inertia is not accounted for), as well as for fast vibrating plates (where inertia of gas is a factor), different damping coefficients can be obtained analytically by solving the Navier-Stokes equation in conjunction with using slip velocity boundary conditions, as shown in the following.

3.5.2.1 Frequency-Independent Damping

One modality of deriving the damping coefficient is expressing the maximum fluid shear stress, which occurs at the fluid–plate boundary:

$$\tau = \mu_{eff}\frac{v_x}{z_0} \tag{3.137}$$

where μ_{eff} is the effective dynamic viscosity and is determined according to various assumptions and contains corrections (mainly in terms of the Knudsen number) that will be discussed a bit later in this section. From Equation (3.137) one can calculate the damping force as:

$$F_d = \tau A = \frac{\mu_{eff} A}{z_0} v_x \tag{3.138}$$

Because this force is equal to the damping coefficient multiplied by velocity, it follows that the damping coefficient is, according to Equation (3.138):

$$c = \frac{\mu_{eff} A}{z_0} \tag{3.139}$$

3.5.2.2 Frequency-Dependent Damping: Stokes Model

For large Reynolds numbers, where inertia effects are larger than viscosity effects, damping is dependent on frequency because gas velocity distribution becomes dependent on time, and different models are in place (Veijola and Turowski [20]). The Navier-Stokes equation, which describes the diffusion problem with no pressure gradient in one dimension, is:

$$\frac{\partial v_x(z,t)}{\partial t} = \upsilon \frac{\partial^2 v_x(z,t)}{\partial z^2} \tag{3.140}$$

where υ is the kinematic viscosity. The generic solution to this partial-derivative differential equation can be obtained in the frequency domain, when the velocity of the plate is:

$$v_x(z,t) = V_x(z)\sin(\omega t) \tag{3.141}$$

It can be shown that the generic amplitude of Equation (3.141) is of the form:

$$V_x(z) = C_1 \sin h\left(\sqrt{\frac{j\omega}{\upsilon}} z\right) + C_2 \cos h\left(\sqrt{\frac{j\omega}{\upsilon}} z\right) \tag{3.142}$$

For fixed boundary conditions, Equation (3.142) reduces to:

$$V_x(z) = V \frac{\sin h\left(\sqrt{\frac{j\omega}{\upsilon}} z\right)}{\sin h\left(\sqrt{\frac{j\omega}{\upsilon}} z_0\right)} \tag{3.143}$$

3.5.2.2.1 Above-the-plate model

The viscous damping coefficient of the motion between an oscillating plate and the unbounded fluid (gas) can be determined by integrating the same Navier-Stokes equation, Equation (3.140). The integration can be performed for fixed boundary conditions (according to the continuum model) or by considering various order slip at the boundaries.

Fixed boundary conditions (continuum model)

For fixed boundary conditions (no velocity slip at the plate interface; see Kundu [21]) the following equations apply:

$$\begin{cases} v_x(0,t) = V_x \cos(\omega t) \\ v_x(\infty,t) = bounded \end{cases} \tag{3.144}$$

Solutions of the type are sought:

$$v_x(z,t) = e^{j\omega t} V_x(z) \tag{3.145}$$

where all the involved functions are complex functions. (It should be mentioned that z is measured from the plate towards the fluid.) By substituting Equation (3.145) into Navier-Stokes Equation (3.140) and by using the two boundary conditions of Equation (3.144), the fluid velocity (which is a real quantity) can be expressed as:

$$v_x(z,t) = v_x e^{-\sqrt{\frac{\omega}{2\upsilon}} z} \operatorname{Re}\left(e^{j\omega t} e^{-(1+j)\sqrt{\frac{\omega}{2\upsilon}} z}\right) = v_x e^{-\sqrt{\frac{\omega}{2\upsilon}} z} \cos\left(\omega t - \sqrt{\frac{\omega}{2\upsilon}} z\right) \tag{3.146}$$

Equation (3.146) resembles the solution to a wave propagation problem, but in actuality there are no restoring forces participating in this motion, and therefore, it represents a diffusion problem (derived from solving the Navier-Stokes original diffusion equation). The amplitude of the fluid motion indicated in Equation (3.146) is:

$$V_x(z) = v_x e^{-\sqrt{\frac{\omega}{2\upsilon}}z} \tag{3.147}$$

and varies with z as shown in Figure 3.30. As z increases the influence of the boundary condition-generated vibration diminishes. For a value of:

$$\delta_d = 4\sqrt{\frac{\upsilon}{\omega}} \tag{3.148}$$

which is known as the *diffusion length* or parameter, the amplitude is:

$$V_x(\delta_d) = V_x(0)e^{-\frac{4}{\sqrt{2}}} = 0.05v_x \tag{3.149}$$

which is 5% of the wall velocity. A parameter similar to the diffusion length is the *penetration depth*, δ, which is the distance where the motion amplitude reduces by a factor of e, which means that:

$$v_x e^{-\sqrt{\frac{\omega}{2\upsilon}}\delta} = v_x e^{-1} \tag{3.150}$$

and therefore:

$$\delta = \sqrt{\frac{2\upsilon}{\omega}} \tag{3.151}$$

The diffusion length and penetration depth are related as:

$$\delta_d = 2\sqrt{2}\delta \tag{3.152}$$

The viscous damping coefficient at the moving plate–fluid interface is found by first determining the shear stress at that interface through application of Newton's law of viscosity (Equation (3.125)). The velocity amplitude derivative at the interface is:

$$\left.\frac{dV_x(z)}{dz}\right|_{z=0} = -v_x\sqrt{\frac{\omega}{2\upsilon}} \tag{3.153}$$

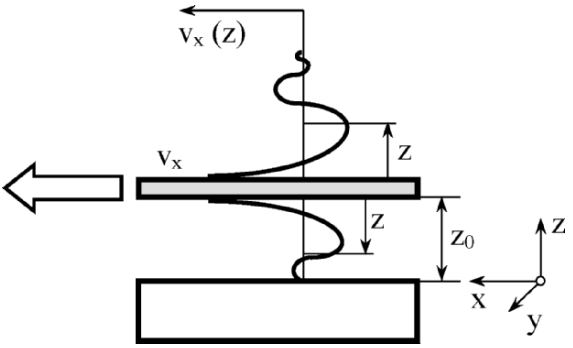

Figure 3.30 Velocities in Stokes slide-film damping

By ignoring the minus sign in Equation (3.153), the shear stress of Equation (3.125) can be expressed, and therefore the corresponding shear force corresponding to the plate surface's A is:

$$F_d = \mu\sqrt{\frac{\omega}{2\upsilon}}Av_x \tag{3.154}$$

A typical viscous damping force is equal to damping coefficient times velocity and, consequently, the damping coefficient is:

$$c_d = \mu\sqrt{\frac{\omega}{2\upsilon}}A = \rho A\sqrt{\frac{\upsilon\omega}{2}} = A\sqrt{\frac{\rho\omega\mu}{2}} \tag{3.155}$$

First-order slip boundary conditions

For rarefied gas, the continuum-model boundary condition at the moving plate needs to be amended, as the gas velocity will differ from the plate's velocity. First-order slip boundary condition (e.g., see Kundu [21]) are expressed as:

$$\begin{cases} v_x(0,t) = V_x - \lambda\left.\dfrac{\partial v_x}{\partial z}\right|_{z=0} \\ v_x(\infty,t) = bounded \end{cases} \tag{3.156}$$

where λ is the free molecular path. By carrying out the procedure that has been detailed for the continuum model, the following gas velocity is found at the moving plate boundary:

$$v_x(z,t) = \frac{v_x}{\lambda\sqrt{\frac{\omega}{2\upsilon}} - 1} e^{-\sqrt{\frac{\omega}{2\upsilon}}z} \cos\left(\omega t - \sqrt{\frac{\omega}{2\upsilon}}z\right) \tag{3.157}$$

The shear stress at the interface is:

$$\tau = \mu \frac{\partial v_x}{\partial x}\bigg|_{z=0} = \frac{\mu\sqrt{\frac{\omega}{2\upsilon}}}{\lambda\sqrt{\frac{\omega}{2\upsilon}} - 1} V_x \tag{3.158}$$

The total force at the gas–plate interface is determined by multiplying the stress of Equation (3.158) by the plate's area. Because the resulting force is the product of plate velocity amplitude V_x by a coefficient, this being the standard form of a damping force, the corresponding damping coefficient is:

$$c = \frac{\mu\sqrt{\frac{\omega}{2\upsilon}}A}{\lambda\sqrt{\frac{\omega}{2\upsilon}} - 1} \tag{3.159}$$

By taking into account that the dynamic viscosity is mass density times kinematic viscosity, the damping coefficient of Equation (3.159) can also be written as:

$$c = \frac{\upsilon\rho A\left(\lambda\omega + \sqrt{2\upsilon\omega}\right)}{\lambda^2\omega - 2\upsilon} \tag{3.160}$$

The penetration depth in this situation is found from its definition equation, namely:

$$\frac{v_x}{\lambda\sqrt{\frac{\omega}{2\upsilon}} - 1} e^{-\sqrt{\frac{\omega}{2\upsilon}}\delta} = v_x e^{-1} \tag{3.161}$$

which results in:

$$\delta = \lambda - \sqrt{\frac{2\upsilon}{\omega}} \tag{3.162}$$

3.5.2.2.2 Between-the-plates model

Again, fixed boundary conditions, as well as slip boundary ones will be considered here.

Fixed boundary conditions (continuum model)

To determine the damping coefficient at the moving plate–fluid interface for the space enclosed between the moving and the fixed plates, a solution to the Navier-Stokes equation is the one suggested by Landau and Lifshitz [19]:

$$v_x(z,t) = \left[A\sin(\beta z) + B\cos(\beta z)\right]e^{-j\omega t} \tag{3.163}$$

where:

$$\beta = (1+j)\sqrt{\frac{\omega}{2\upsilon}} \tag{3.164}$$

and z is the variable length parameter that ranges within the [0, z_0] interval, and is measured from the mobile plate (when $z = 0$), as suggested in Figure 3.30. By using the continuum-model (no-slip) boundary conditions of this problem:

$$\begin{cases} v_x(0) = V_x e^{-j\omega t} \\ v_x(z_0) = 0 \end{cases} \tag{3.165}$$

where the first boundary condition used the complex-number notation to denote the mobile plate velocity, the space-dependent portion of Equation (3.163) becomes:

$$v_x(z) = V_x \frac{\sin\left[\beta(z_0 - z)\right]}{\sin(\beta z)} \tag{3.166}$$

The shear stress at the moving plate–fluid interface is found by using Newton's law as:

$$\tau = \mu \left.\frac{dv_x(z)}{dz}\right|_{z=0} = \mu\beta V_x \cot(\beta z_0) \tag{3.167}$$

Equation (3.167) gives the complex number form of the shear stress, but only its real part accounts for the actual shear stress, which is:

$$\tau = \mu\beta_1 V_x \frac{\sin h\left(2\beta_1 z_0\right) + \sin\left(2\beta_1 z_0\right)}{\cos h\left(2\beta_1 z_0\right) - \cos\left(2\beta_1 z_0\right)} \tag{3.168}$$

with:

$$\beta_1 = \sqrt{\frac{\omega}{2\upsilon}} \tag{3.169}$$

Because, again, the damping force is shear stress times area but is also damping coefficient times velocity, the damping coefficient can be computed from Equation (3.167) as:

$$c = \mu\beta A \frac{\sin h\left(2\beta_1 z_0\right) + \sin\left(2\beta_1 z_0\right)}{\cos h\left(2\beta_1 z_0\right) - \cos\left(2\beta_1 z_0\right)} \tag{3.170}$$

Example 3.16

Evaluate the total damping coefficient generated due to air friction above plate that undergoes vibrations parallel to the substrate, as well as between the plate and the substrate, by considering the continuum model does apply (with fixed boundary conditions).

Solution:

Equations (3.155) and (3.170) give the damping coefficients outside the plate and between the plate and the substrate, respectively. The total loss in case several independent effects superimpose can be evaluated by means of the inverse of an equivalent *Q*-factor, which is obtained by adding up the inverses of the individual *Q*-factors, as shown by Equation (3.44). At the same time, according to Equation (3.24), the *Q*-factor is proportional to the inverse of the damping coefficient. Consequently, the total damping coefficient is the sum of individual contributions from above-the-plate and between-the-plates damping coefficients, namely:

$$c = c_a + c_b \tag{3.171}$$

where c_a is given in Equation (3.155) and c_b in Equation (3.170). The plot of Figure 3.31 shows the variation of the c_a/c ratio.

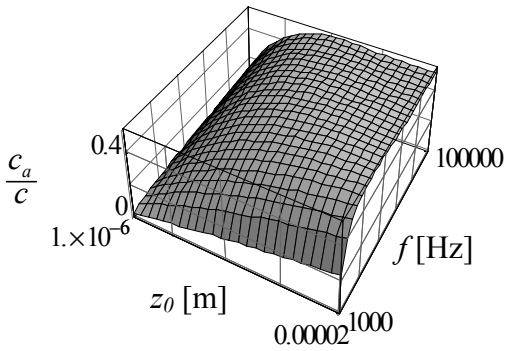

Figure 3.31 Above-the-plate damping coefficient as a fraction of the total damping coefficient

For relatively small gaps and driving frequencies, the damping produced above the plate is less significant in the overall damping coefficient, as shown in the figure, cases in which the damping owing to fluid–structure interaction predominates. For higher gaps and frequencies, the fraction of damping produced above the plate increases and approaches the one generated between the plates.

First-order slip boundary conditions

The model described in the previous subsection together with its corresponding damping coefficient equation account for fixed boundary conditions, according to the continuum model. When slip boundary conditions are assumed (which account for flows in the slip and/or transition flow regimes), a different coefficient is produced, as shown next.

The *slip boundary conditions* account for gas rarefaction at low pressures and very small gaps that result in a gas velocity that is non-zero at the fixed wall (the slip velocity) and is different from the oscillating wall velocity at that interface. These changes in fluid velocity distribution alter the damping coefficient resulting from the rarefied fluid-moving plate interaction. The *first-order slip boundary conditions* (Burgdorfer [22]), also known as Maxwell's boundary conditions, are:

$$\begin{cases} v_x(0) = \lambda \left.\dfrac{\partial v_x}{\partial z}\right|_{z=0} \\ v_x(z_0) = V_x - \lambda \left.\dfrac{\partial v_x}{\partial z}\right|_{z=z_0} \end{cases} \tag{3.172}$$

where v_x is the gas slip velocity (at either the fixed plate or the oscillating one), V_x is the plate velocity amplitude, λ is the mean free molecular path,

and z is measured starting from the fixed plate. This model considers the velocity distribution near the surface as being linear.

If the solution of Equation (3.142) to the Navier-Stokes equation (Equation (3.140)) is used, the two constants involved are determined by using the slip boundary conditions of Equation (3.172). By then using the normal procedure of expressing the real part of the complex velocity distribution, followed by calculation of its z-dependent first derivative and calculation of the shear stress at the moving plate–fluid interface, the damping force is obtained by multiplying the shear stress by the plate's surface area. This last step enables identifying the viscous damping coefficient as the multiplier of the plate's velocity amplitude. The viscous damping coefficient, as shown by Veijola and Turowski [20], for instance, is:

$$c = \mu\beta_1 A \frac{\sin\mathrm{h}\left(2\beta_1 z_0\right) + \sin\left(2\beta_1 z_0\right) + c_1}{\cos\mathrm{h}\left(2\beta_1 z_0\right) - \cos\left(2\beta_1 z_0\right) + c_2} \tag{3.173}$$

where the two terms, c_1 and c_2, are the additions to the damping coefficient corresponding to non-slip boundary conditions (Equation (3.170)) and are, according to Veijola and Turowski [20]:

$$\begin{cases} c_1 = 4\beta_1\lambda\left[\left(1+\beta_1^2\lambda^2\right)\cos\mathrm{h}\left(2\beta_1 z_0\right) + \left(1-\beta_1^2\lambda^2\right)\cos\left(2\beta_1 z_0\right)\right] \\ \quad + 6\beta_1^2\lambda^2\left[\sin\mathrm{h}\left(2\beta_1 z_0\right) - \sin\left(2\beta_1 z_0\right)\right] \\ c_2 = 4\beta_1\lambda\left[\left(1+2\beta_1^2\lambda^2\right)\sin\mathrm{h}\left(2\beta_1 z_0\right) + \left(1-2\beta_1^2\lambda^2\right)\sin\left(2\beta_1 z_0\right)\right] \\ \quad + 4\beta_1^2\lambda^2\left[\left(2+\beta_1^2\lambda^2\right)\cos\mathrm{h}\left(2\beta_1 z_0\right) - \left(2-\beta_1^2\lambda^2\right)\cos\left(2\beta_1 z_0\right)\right] \end{cases} \tag{3.174}$$

Higher-order Slip Boundary Conditions

The first-order boundary slip model captures the linear velocity distribution at boundaries for vibration frequencies that are not so high. In the case of higher frequencies, the linear character of velocity distribution near the oscillating plate needs to be replaced by a higher-order distribution. A second-order slip boundary condition, as shown by Beskok and Karniadakis [23], Beskok et al. [24], Bahukudumbi et al. [25], Park et al. [26] or Veijola and Turowski [20], requires:

$$\begin{cases} v_x(0) = \lambda \left.\dfrac{\partial v_x}{\partial z}\right|_{z=0} \\ v_x(z_0) = V_x - \dfrac{\lambda}{1-b\lambda} \left.\dfrac{\partial v_x}{\partial z}\right|_{z=z_0} \end{cases} \tag{3.175}$$

where the higher-order factor, according to Beskok and Karniadakis [23], is computed as:

$$b = \frac{\left.\frac{\partial^2 v_x}{\partial z^2}\right|_{z=z_0}}{2\left.\frac{\partial v_x}{\partial z}\right|_{z=z_0}} \tag{3.176}$$

where v_x was selected to be the velocity distribution according to the continuum model (Equation (3.146)). For $b = 0$, Equation (3.175) is identical to Equation (3.172), which describes the first-order slip model. By applying the same procedure indicated to the first-order slip model, the damping coefficient can be obtained. Veijola and Turowski [20] propose the following complex number form damping coefficient:

$$c = \frac{\mu A \beta_2 \left[2 + \beta_2 \lambda \tanh\left(\beta_2 z_0\right) - \beta_2^2 \lambda^2 \tanh^2\left(\beta_2 z_0\right)\right]}{4\beta_2 \lambda + \left(2 + \beta_2^2 \lambda^2\right)\tanh\left(\beta_2 z_0\right) - \beta_2 \lambda \tanh^2\left(\beta_2 z_0\right)} \tag{3.177}$$

where $\beta_2 = (2j\beta_1)^{1/2}$. A variant of modeling higher-order slip velocity boundary conditions at the moving wall is proposed by Bahukudumbi et al. [25], who propose the following boundary condition:

$$\begin{cases} v_x(0) = \lambda \left.\frac{\partial v_x}{\partial z}\right|_{z=0} \\ v_x(z_0) = V_x - \alpha\lambda \left.\frac{\partial v_x}{\partial z}\right|_{z=z_0} \end{cases} \tag{3.178}$$

where α is the slip coefficient, which is expressed, according to the same reference, as:

$$\alpha = 1.2977 + 0.71851 \tan^{-1}\left[-1.17488\left(\frac{\lambda}{z_0}\right)^{0.58642}\right] \tag{3.179}$$

For a slip coefficient of $\alpha = 1$, the classical Maxwell, first-order slip velocity boundary condition is retrieved.

3.5.3 Free Molecular Flow Regime and Unifying Theories

For very large Knudsen numbers, *Kn*, the free molecular path exceeds by far the gap dimensions, and the flow is in the free regime. The shear stress on a plate that displaces at a velocity V_x can be expressed, according to Kogan [27], for instance, as:

$$\tau_\infty = \rho_0 V_x \sqrt{\frac{2RT}{\pi}} \tag{3.180}$$

where R is the universal gas constant and T is the temperature of the mobile plate. The damping coefficient corresponding to the free molecular flow regime is therefore:

$$c_\infty = \rho_0 A \sqrt{\frac{2RT}{\pi}} \tag{3.181}$$

Attempts have been made by researchers in this domain to generate closed-form analytical equations that would be applicable for the whole range of Knudsen numbers, covering the domain from continuum to free molecular. Corrections expressing slip-wall effects can be incorporated in effective values of either the shear stress or the dynamic viscosity, and therefore the simple linear Couette model can be used to generate damping coefficients by means of Equations (3.129), (3.130), and (3.131) at the beginning of this section treating the slide-film damping.

Veijola and Turowski [20], for instance, suggest using the following effective damping coefficient:

$$\mu_{eff} = \frac{\mu}{1 + 2\dfrac{\lambda}{z_0}} \tag{3.182}$$

where μ is the actual dynamic viscosity and λ is the free mean molecular path. The same reference proposes as an alternative a different effective dynamic viscosity, which is derived from normalizing the shear stress by the free molecular path as:

$$\mu_{eff} = \frac{\mu}{1 + 2K_n + 0.2K_n^{0.788} e^{-0.1K_n}} \tag{3.183}$$

which represents a curve fit obtained from numerical results of an integro-differential equation derived by Cercignani and Pagani [28] based on a

linearized Boltzmann equation. First-order slip boundary conditions have been taken into account in these models. Having the effective dynamic viscosity enables calculation of the shear stress by means of Newton's law (Equation (3.125)). Similarly, Bahukudumbi et al. [25] propose the following shear stress ratio obtained from curve fitting of numerical results:

$$\frac{\tau}{\tau_\infty} = \frac{a\left(Kn\right)^2 + 2bKn}{a\left(Kn\right)^2 + cKn + b} \tag{3.184}$$

where a = 0.530, b = 0.603, c = 1.628 (values rounded to three decimal points). Equation (3.184) enables expressing the shear stress for any value of the Knudsen number, from 0 (continuum model) to infinity (free molecular regime). The damping force is obtained by multiplying the shear stress by the moving plate area, which enables determining the damping coefficient.

3.6 THERMOELASTIC DAMPING

The coupling between a strain/deformation field in an elastic body and the temperature field is best illustrated by the equation connecting the elongation of a bar, Δl, to the temperature variation, ΔT as:

$$\Delta l = \alpha l \Delta T \tag{3.185}$$

by means of the linear coefficient of thermal expansion α. An oscillating elastic body is out of equilibrium state, but local variations of its strain field interact with the thermal variations, according to Equation (3.185). This connection provides a mechanism for energy dissipation towards regain of equilibrium. This is actually a relaxation process consisting of an irreversible heat flow. For a vibrating beam, for instance, where the upper fibers contract and the lower fibers extend at a given moment in time, a heat flow loss occurs from the heated fibers (the extended ones) to the cooled fibers (the ones that contract). This energy loss phenomenon is known as TED.

Roszhart [29] derived a model for cantilever beams which predicts the following Q-factor:

$$Q = \frac{16\omega^2 t^4 c^2 \rho^2 + \kappa^2}{4\omega t^2 \alpha^2 \kappa E T} \tag{3.186}$$

where c is the specific heat, κ is the heat capacity, E is Young's modulus, ρ is the mass density, T is the temperature, t is the thickness, and ω is the vibration frequency.

In the 1930s, Zener [30] proposed an approximation to the *Q*-factor pertaining to thermoelastic losses, which is still considered operationally valid. Zener's model, also known as the *standard model of the anelastic solid*, considers that damping can be approximated by a relaxation process in which thermal diffusion occurs across the thickness of a vibrating beam. The standard model has at its core a generalization of Hooke's law, which is expressed as:

$$\sigma + \tau_{\varepsilon} \frac{d\sigma}{dt} = E_r \left(\varepsilon + \tau_{\sigma} \frac{d\varepsilon}{dt} \right) \tag{3.187}$$

where E_r is the relaxed modulus of elasticity, whereas τ_{ε} and τ_{σ} are the constant-strain relaxation time and constant-stress time, respectively. By assuming that the stress and strains vary harmonically, which in complex notation is:

$$\begin{cases} \sigma = \sigma_0 e^{j\omega t} \\ \varepsilon = \varepsilon_0 e^{j\omega t} \end{cases} \tag{3.188}$$

Equation (3.187) becomes:

$$\sigma_0 = E_{r,c} \varepsilon_0 \tag{3.189}$$

which is similar to the normal Hooke's law and where $E_{r,c}$ is a complex modulus, expressed as:

$$E_{r,c} = E_r \frac{1 + j\omega\tau_{\sigma}}{1 + j\omega\tau_{\varepsilon}} \tag{3.190}$$

The inverse of the *Q*-factor can be defined as the ratio of the imaginary part to the real part of the complex modulus, and after transforming the complex modulus of Equation (3.190) in its standard, complex-number form:

$$E_{r,c} = \frac{1 + \omega^2 \tau_{\sigma} \tau_{\varepsilon}}{1 + \omega^2 \tau_{\varepsilon}^2} + j \frac{\omega\left(\tau_{\sigma} - \tau_{\varepsilon}\right)}{1 + \omega^2 \tau_{\varepsilon}^2} \tag{3.191}$$

the inverse of the *Q*-factors can be expressed as:

$$Q^{-1} = \frac{E_u - E_r}{\sqrt{E_u E_r}} \times \frac{\omega_r \tau_{th}}{1 + \left(\omega_r \tau_{th}\right)^2} \tag{3.192}$$

E_u is the unrelaxed modulus and is defined as:

$$E_u = \frac{\tau_\sigma}{\tau_\varepsilon} E_r \tag{3.193}$$

where the *thermal relaxation time* is:

$$\tau_{th} = \frac{t^2 \rho c}{\pi^2 k} \tag{3.194}$$

with c being the specific heat (at either constant pressure or constant volume [the differences are small between the two conditions]), ω_r being the cantilever resonant frequency, T being the temperature, t being the cantilever cross-sectional thickness, ρ being the mass density, and k being the thermal conductivity.

The Q-factor accounting for thermal damping losses, according to Zener's model and when considering the following approximation (Lifshitz and Roukes [31]):

$$\frac{E_u - E_r}{\sqrt{E_u E_r}} \approx \frac{E_{ad} - E}{\sqrt{E^2}} = \frac{E\alpha^2 T}{c} \tag{3.195}$$

is:

$$Q = \frac{c}{E\alpha^2 T} \times \frac{1 + \left(\omega_r \tau_{th}\right)^2}{\omega_r \tau_{th}} \tag{3.196}$$

In Equation (3.195), E_{ad} is the adiabatic (unrelaxed) modulus of elasticity, whereas E is the regular, isothermal (relaxed) modulus of elasticity.

Example 3.17

Analyze the Q-factor due to thermal damping in terms of the relaxation constant $\omega_r \tau_{th}$.

Solution:

The inverse of the Q-factor, Q^{-1}, which is proportional to the losses incurred by a system, is plotted in a non-dimensional form, as shown in Figure 3.32, based on Equation (3.196). As Figure 3.32 shows, the non-dimensional damping has a maximum for $\omega_r \tau_{th} = 1$, which indicates that the resonant frequency and the relaxation rate (the inverse of the relaxation time) should be approximately equal for the maximum peak damping to occur.

When $\omega_r >> 1/\tau_{th}$, the material does not have the necessary time to relax because the vibration is too fast. When, on the contrary, $\omega_r << 1/\tau_{th}$, the vibration is very slow and the system is in equilibrium technically, with little energy being lost.

Lifshitz and Roukes [31] derived the exact closed-form solution to the Q-factor corresponding to a thin cantilever by using the equations of linear thermoelasticity:

$$Q = \frac{c\zeta^2}{6E\alpha^2 T}\left[1 - \frac{\sinh\zeta + \sin\zeta}{\zeta\left(\cosh\zeta + \cos\zeta\right)}\right]^{-1} \tag{3.197}$$

with:

$$\xi = t\sqrt{\frac{\omega_r \rho c}{2k}} \tag{3.198}$$

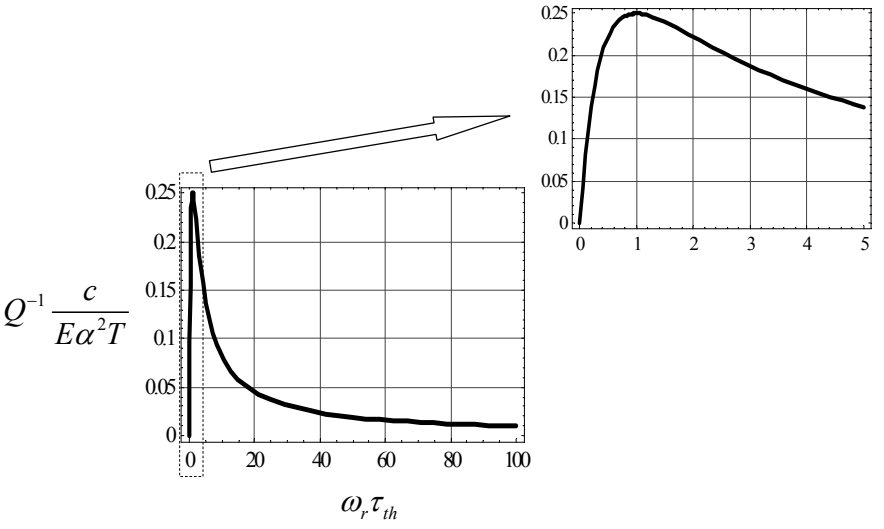

Figure 3.32 Non-dimensional thermal damping as a function of the relaxation parameter

3.7 OTHER INTRINSIC LOSSES

Other intrinsic losses are *phonon-mediated* and they include the ones produced by phonon–electron interactions as well as those generated by the interaction between phonons and the mechanical vibration of a microdevice. The first category of losses is a viscous drag exerted by the free electrons on

oscillating ions and is mostly significant in metallic MEMS because it is based on material high electrical conductivity (Czaplewski et al. [32]).

The latter loss category is defined by the propagating mechanical vibration in a MEMS device, which causes the phonons to thermally readjust and reach a different equilibrium state, this state alteration being the channel for energy losses. The *Q*-factor in this case (Czaplewski et al. [32]) is of the Zener type, namely:

$$Q = \frac{\rho v_l^2}{CT\gamma^2} \times \frac{1 + \left(\omega_r \tau_{ph}\right)^2}{\omega_r \tau_{ph}} \tag{3.199}$$

where C is the heat capacity per unit volume, v_l is the longitudinal wave (sound) velocity and the phonon relaxation time is:

$$\tau_{ph} = \frac{3\kappa}{\rho C_p v_D^2} \tag{3.200}$$

κ being the material thermal conductivity, C_p being the constant-pressure heat capacity, and v_D being the Debye sound velocity defined as:

$$v_D = v_l v_t \sqrt[3]{\frac{3}{2v_l^3 + v_t^3}} \tag{3.201}$$

It is known that the longitudinal velocity is:

$$v_l = \sqrt{\frac{E}{\rho}} \tag{3.202}$$

whereas the transverse wave velocity (or the group velocity) is:

$$v_t = \frac{\lambda}{T} = \frac{\lambda\omega}{2\pi} \tag{3.203}$$

The constant γ in Equation (3.199) is the *Gruneisen's constant* (e.g., see Braginski et al. [33] and Burakowsky and Preston [34]), whose definition is:

$$\gamma = \frac{\alpha E}{\rho C_v} \tag{3.204}$$

Burakowsky and Preston [34] propose the following equation to determining γ, which depends only on material density:

$$\gamma = \frac{1}{2} c_1 \rho^{1/3} + c_2 \rho^{c_3} \tag{3.205}$$

where c_1, c_2, and c_3 are constants that can be evaluated individually for various materials, and the same reference gives those values for 20 metallic materials.

Another internal dissipation mechanism is due to *defects* or *disorder* in a material, and relaxation (damping) is provided by reconfiguration/reordering between equilibrium states that usually occurs through motion by atoms, vacancies, impurities, or dislocations. The *Q*-factor of a MEMS oscillator subjected to this particular type of loss is of the generic Zener-type, namely:

$$Q = c \frac{1 + (\omega_r \tau)^2}{\omega_r \tau} \tag{3.206}$$

where the constant c depends on the type of defect and its intensity. The relaxation time (Czaplewski et al. [32]) can be expressed for these processes as an Arrhenius-type equation:

$$\frac{1}{\tau} = \frac{1}{\tau_0} e^{-\frac{E_a}{RT}} \tag{3.207}$$

where R is the universal gas constant (R = 8.31 J/(mol K)), τ_0 is the characteristic atomic vibration period and is of the order of 10^{-13} s, and E_a is the activation energy of the relaxation process. Usually this energy is equal to the self-diffusion energy and is of the order of 1–2 eV per mol.

Example 3.18

Evaluate the relaxation time involved in the losses due to defect motion if the characteristic atomic vibration period is $\tau_0 = 2.5 \times 10^{-13}$ s and the activation energy is E_a = 1.5 eV. Considering a microresonator whose resonant frequency is 10,000 Hz is defined by a *Q*-factor Q = 1000, which is solely due to defect motion losses, determine the constant c of Equation (3.206).

Solution:

By taking into account that 1 eV = 1.6×10^{-9} J and by considering the numerical data of this problem, the relaxation time can be expressed as a function of temperature, and Figure 3.33 plots this relationship. As Figure 3.33 indicates, the relaxation time decreases when the temperature increases, as expected, but is largely determined by the value of the characteristic atomic vibration period τ_0. The constant c is simply found from Equation (3.206) as:

$$c = \frac{2\pi f_r \tau}{1+\left(2\pi f_r \tau\right)^2} Q \tag{3.208}$$

and its numerical value is $c = 6.28 \times 10^{-6}$.

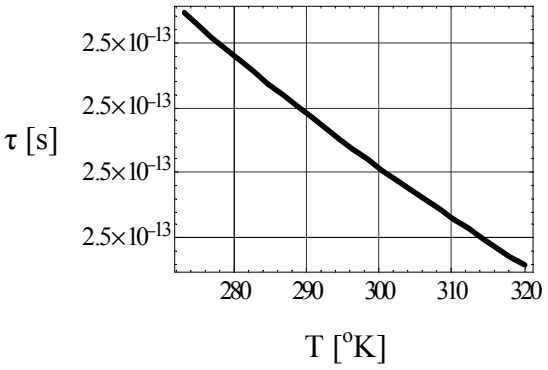

Figure 3.33 Relaxation time as a function of temperature

3.8 SUBSTRATE (ANCHOR) LOSSES

Vibration of micro/nano mechanical devices, particularly the resonant ones, is transmitted to the substrate and dissipates into it; the corresponding losses are known as support (or substrate, or anchor) losses. Reduction of these losses, as indicated by Mihailovich and MacDonald [35], for instance, can be achieved by either utilizing symmetry in designing resonant structures such that zero (desirably) forces/moments are transmitted to the support or by interposing a mass between the oscillating structure and the substrate such that the energy of the mass is small compared to the energy of the original structure.

Modeling and quantifying losses to the substrate by a micro/nano oscillator is generally performed by assessing the vibration energy, which is transmitted through the anchor regions by the shearing forces and bending or torsional moments generated locally by the vibrating structures. Park and Park [36] developed a methodology enabling evaluation of the anchor losses by means of a modified Fourier semi-analytic technique involving numeric solutions. Osaka et al. [37] considered cantilever beams of infinite width that are attached to a semi-infinite substrate and gave the following Q-factor corresponding to anchor losses:

$$Q \approx 2.17 \frac{l^3}{t^3} \tag{3.209}$$

where l is the beam length and t is its thickness. Hao et al. [38] derived a very similar Q-factor, namely:

$$Q \approx 2.09 \frac{l^3}{t^3} \tag{3.210}$$

value corresponding to the first vibration mode and to a material with Poisson's ratio $\mu = 0.3$. The same reference developed an equation requiring numeric integration, which gives the Q-factor of cantilevers for various modes as a function of modal amounts and the Poisson's ratio. The respective equation indicates the Q-factor decreases with the mode number increasing and is proportional to the cube of the length-to-thickness ratio. A similar result is provided by the same referenced paper for bridges (clamped-clamped beams).

Photiadis and Judge [39] proposed a model with closed-form Q-factor of cantilevers by taking into account all the dimensions of the beam together with the substrate thickness. For the case in which the substrate thickness t_s is smaller than the wavelength of the wave transmitted to the substrate, they derived the following Q-factor equation:

$$Q = 1.05 \frac{l}{w} \times \frac{t_s^2}{t^2} \tag{3.211}$$

where, in addition to the parameters already introduced here, w is the beam cross-sectional width. Equation (3.211) is a simplification of a more generic equation derived in the same reference—the equation mentioned here corresponds to cantilever designs with thicknesses far smaller than the substrate thickness and was shown valid for cases when $\lambda_s/3 < t_s < \lambda_s$. Figure 3.34 shows the dependency of the Q-factor on the l/w and t_s/t ratios.

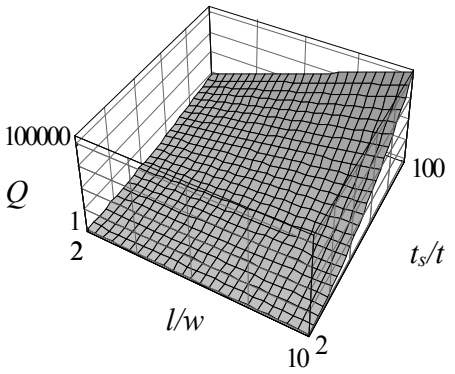

Figure 3.34 Quality factor due to anchor losses in terms of geometry

Example 3.19

Design a cantilever that would be able to produce an anchor loss-related Q-factor of Q = 10,000 when the substrate has a thickness t_s = 500 μm.

Solution:

Equation (3.211) enables expression of the cantilever thickness as:

$$t = 1.025\sqrt{\frac{1}{Q}\times\frac{l}{w}}\,t_s \tag{3.212}$$

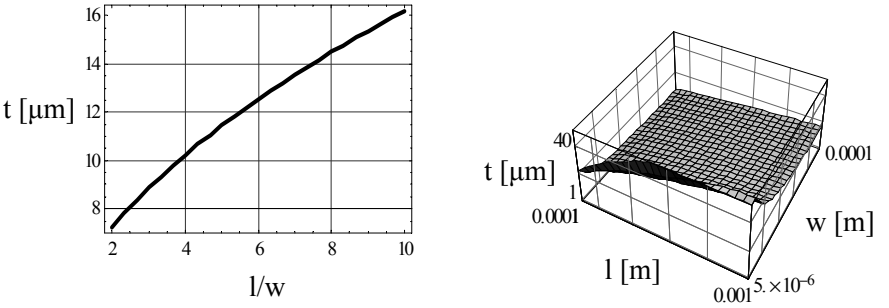

Figure 3.35 Cantilever thickness in terms of length and width

For the numerical data of the problem, the solution is: t = 5.125 $(l/w)^{1/2}$. The thickness is plotted in terms of the cantilever length and cross-sectional width in Figure 3.35. As Figure 3.35 shows it, the thickness increases with the length-to-width ratio for the specified values of the Q-factor and substrate thickness. For l/w = 5, the cantilever thickness becomes: t = 11.6 μm.

Photiadis and Judge [39] also analyzed designs for which the substrate thickness is larger compared to the wavelength of the transmitted vibration, and proposed the following Q-factor:

$$Q = 3.226\frac{l}{w}\times\frac{l^4}{t^4} \tag{3.213}$$

Both Equations (3.211) and (3.213) were derived for a material with μ = 3 (steel-type). It can be seen from Equation (3.213) that the substrate thickness does not affect the Q-factor for relatively thick substrates. There are also marked differences between the predictions of Equation (3.209) by Osaka et al. [37], Equation (3.210) by Hao et al. [38], on one side, and Equation (3.213) by Photiadis and Judge [39].

3.9 SURFACE LOSSES

The generic Zener model can also stand for dissipative processes different from the TED since by taking into account a complex modulus of the type:

$$E_c = E_1 + jE_2 \tag{3.214}$$

where E_1 can be the real, conventional elastic modulus of a specific material, and E_2 stands for the dissipative part of that material (generated by lattice defects motion, for instance), the Q-factor is simply:

$$Q = \frac{\mathrm{Re}(E_c)}{\mathrm{Im}(E_c)} = \frac{E_1}{E_2} \tag{3.215}$$

Equation (3.215) can actually be derived for the case of internal bulk (through the volume) dissipation (e.g., as shown by Yasumura et al. [40]) by expressing the Q-factor according to its definition, which takes into account the energy stored and the energy lost during one oscillation cycle. According to Equation (3.215), the Q-factor related to bulk internal losses strictly depends on elastic and dissipative material properties.

Surface loss mechanisms can also occur in situations such as disruption of the atomic lattice produced by microfabrication defects, for instance, or in cases of surface contamination (such as adsorbates on the surface). Yasumura et al. [40] derived the following Q-factor owing to surface losses for a cantilever having the cross-sectional width w and thickness t:

$$Q = \frac{wt}{2\delta\left(3w+t\right)} \times \frac{E_1}{E_{s,1}} Q_s \tag{3.216}$$

where δ is the thickness of a thin dissipative layer for which the following complex modulus is used:

$$E_{s,c} = E_{s1} + jE_{s2} \tag{3.217}$$

defined by a Q-factor:

$$Q_s = \frac{E_{s1}}{E_{s2}} \tag{3.218}$$

For cantilevers with large widths compared to their thickness, $w >> t$, Equation (3.216) simplifies to:

$$Q = \frac{t}{6\delta} \times \frac{E_1}{E_{s,1}} Q_s \tag{3.219}$$

As indicated by Equations (3.216) and (3.219), the surface losses are affected by the cross-sectional dimensions, in addition to elastic and dissipative material properties, and are not influenced by the cantilever length, as one would expect by taking into account that length defines the longitudinal area, $w \times l$.

Problems

Problem 3.1

The differential equation expressing the free damped vibrations of a single DOF microresonator is: $\ddot{x} + 20\dot{x} + 1,000,000x = 0$. Determine the mass m, damping coefficient c, and stiffness k, as well as the damped resonant frequency ω_d of this lumped-parameter system.

Problem 3.2

Repeat Problem 3.2 in the case of the following differential equation: $\ddot{x} + 500\dot{x} + 6,250,000x = 0$.

Problem 3.3

The free damped vibrations of a two DOF mechanical microsystem are characterized by the following mass, damping and stiffness matrices: $[M] = \begin{bmatrix} a & 0 \\ 0 & a \end{bmatrix}; [C] = \begin{bmatrix} b & 0 \\ 0 & b \end{bmatrix}; [K] = \begin{bmatrix} d_1 & -d_2 \\ -d_2 & d_1 \end{bmatrix}$, where the real coefficients a, b, d_1, and d_2 are specified. Identify a mechanical microsystem that possesses these properties by drawing a schematic of the microsystem and by also calculating its individual physical parameters.

Problem 3.4

Repeat Problem 3.3 in the case the microsystem's matrices are: $[M] = \begin{bmatrix} a & 0 \\ 0 & a \end{bmatrix}; [C] = \begin{bmatrix} b & 0 \\ 0 & b \end{bmatrix}; [K] = \begin{bmatrix} d_1 & -d_2 \\ -d_2 & d_1 \end{bmatrix}$.

Problem 3.5

The free damped response of the mechanical microfilter of Figure 3.36 is determined experimentally, consisting of the logarithmic decrements δ_1 and δ_2, and the two damped resonant frequencies ω_{d1} and ω_{d2}. By also knowing the mass m of the two rigid oscillators, evaluate the stiffnesses k_1 and k_2.

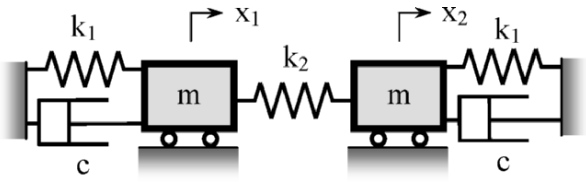

Figure 3.36 Two DOF microfilter with damping

Problem 3.6

Calculate the bending resonant frequency ω_r of a resonator for which the logarithmic decrement δ and damped frequency ω_d are known.

Problem 3.7

A paddle microcantilever is tested at resonance by using out-of-the-plane bending and torsion. It is determined the torsion-to-bending damped resonant frequency ratio is r. By using a lumped-parameter model, evaluate the overall losses corresponding to these motions. By using a lumped-parameter model, evaluate the loss corresponding to torsion as a function of the loss produced through bending.

Problem 3.8

Solve Problem 3.7 by considering a paddle microbridge instead of a paddle microcantilever.

Problem 3.9

A paddle microcantilever is tested at resonance by monitoring its damped, out-of-the-plane response. The resonant Q-factor Q_r and the damped resonant frequency ω_d are determined experimentally. By knowing all geometric and inertia parameters of the microbridge, use a lumped-parameter model (with the paddle rigid and the root massless and compliant) to evaluate the elasticity (Young's) modulus E of the microbridge material.

Problem 3.10

Solve Problem 3.9 by considering a paddle microbridge instead of a paddle microcantilever.

Problem 3.11

Establish a relationship between the resonant (forced) Q-factor and the free-response Q-factor (with non-zero initial velocity) for a single DOF damped microresonator when the logarithmic decrement δ is known.

Problem 3.12

A constant rectangular cross-section microbridge with E = 155 GPa, ρ = 2300 kg/m^3 and length l = 100 μm is displaced by 5 μm at its midpoint and then let to freely vibrate. After t = 50 s, its midpoint vibration amplitude is 30 nm. Evaluate the Q-factor corresponding to the overall losses.

Problem 3.13

A paddle microcantilever with both segments contributing to compliance and inertia is vibrated in out-of-the-plane bending in a vacuum environment to evaluate structural losses, and the corresponding Q-factor is determined experimentally. By ignoring other losses of this microsystem, and by considering all geometric and material parameters of the microbridge are known, calculate the structural loss coefficient α.

Problem 3.14

A Q-factor of 7,800 is experimentally determined for a trapezoid cantilever whose minimum width, maximum width, thickness, and length are 20 μm, 80 μm, 1 μm, and 300 μm, respectively. The structural damping roughly represents 80% of the total losses. Determine the elastic modulus of this cantilever's material. It is also known that α = 0.0005.

Problem 3.15

A microbridge formed of a central plate of 90 μm length, 10 μm width, and 1 μm thickness, and two side CNTs, each 20 μm long and 50 nm in diameter, vibrates normally to the substrate. Knowing the bridge–substrate initial gap is 3 μm and that the Q-factor owing to squeeze-film damping is 9,300, calculate the dynamic viscosity. Known are also ω = 6000 rad/s and E = 50 GPa. Use Zhang's continuum-gas model.

Problem 3.16

A 300 μm × 50 μm × 2 μm plate vibrates normal to the substrate at 10 kHz. The plate is supported by two end rectangular cross-section beams, each 50 μm long, 10 μm wide, and 1 μm thick. The initial gap is 12 μm, the gas pressure is 0.001 atm, and the dynamic viscosity is 1.8×10^{-5} N-s/m^2. Calculate the squeeze-film damping coefficient.

Problem 3.17

A plate 200 μm long and 40 μm wide is used to determine the nature of an unknown gas by monitoring the plate's vibratory response against a substrate (the initial gap is 8 μm). The plate vibrates at 8,000 Hz at normal temperature and pressure. Considering the Q-factor corresponding to squeeze-film damping is 7,600, calculate the molecular mass of the gas.

Problem 3.18

The plate shown in Figure 3.37 is supported by two CNT beams and can vibrate in out-of-the-plane translation and rotary motion. Knowing that $l = 400$ μm, $w = 70$ μm, $l_b = 300$ μm, $d = 60$ nm (d is the CNT diameter), and also that the Q-factors owing to squeeze-film damping are $Q_t = 6{,}500$ for translation and $Q_r = 6{,}800$ for rotation, find the plate-substrate gap z_0 and the dynamic viscosity μ. Known is also that $f_t = f_r = 100$ Hz.

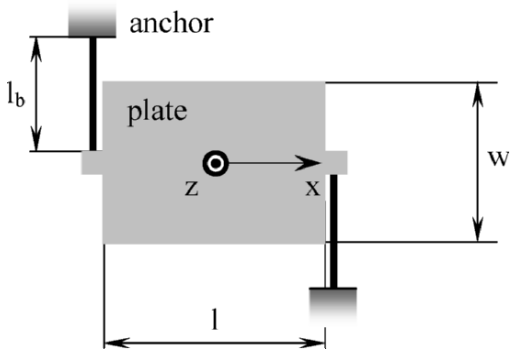

Figure 3.37 Bridge suspended on two carbon nanotube beams

Problem 3.19

A microresonator consists of a central square plate (of known mass m and dimensions $L \times L$), which is supported symmetrically on the midpoints of its sides by four identical CNT beams of known length l, diameter d, and modulus of elasticity E. At a very small pressure p, this microsystem can be used as a thermal sensor. The out-of-plane vibrations of the plate are monitored experimentally and the Q-factor Q is determined at $\omega = \omega_r$. By using Bao's molecular-flow model, and by also knowing the gas molecular mass M_m and the gas constant R, determine the gas temperature T.

Problem 3.20

A torsional micromirror is formed of a rectangular plate and two end beams. The inertia and geometric properties of the plate and beams are known. Compute the equivalent viscous damping ratio when the Q-factor corresponding to torsional vibrations of the micromirror is known. Consider only the losses produced through squeeze-film damping.

Problem 3.21

A paddle microbridge with the paddle rigid and the root segments massless and compliant (of constant rectangular cross-section) is used as a torsional oscillator to assess the dynamic viscosity coefficient μ of an unknown gas. All design and material properties being known, as well as the damped resonant frequency ω_d and resonant quality factor Q_r, devise an algorithm to determine μ. Known is also that $f_t = f_r = 100$ Hz.

Problem 3.22

Find the damped resonant frequency of the plate with 10 holes, as shown in Figure 3.38, by considering the squeezed-film stiffness. The plate is suspended by two end springs, each of 2 N/m stiffness. Known are the hole radius $r = 3$ μm, $l = 80$ μm, $w = 20$ μm, $p = 15$ μm, and $\mu = 1.7 \times 10^{-5}$ N-s/m^2, $z_0 = 8$ μm, $t = 2$ μm and $\rho = 2300$ kg/m^3.

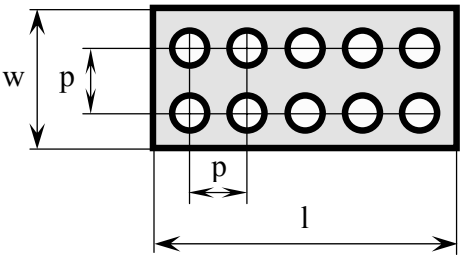

Figure 3.38 Plate with holes

Problem 3.23

Study the variation of c in Problem 3.22 as a function of the number of holes n.

Problem 3.24

A plate vibrates parallel to the substrate by maintaining a constant gap of 10 μm. The air density is $\rho = 1.1$ kg/m^3 and the dynamic viscosity is $\mu = 1.7 \times 10^{-5}$ N-s/m^2. By using the continuum model, determine the frequency at which the damping coefficient corresponding to the above-the-plate fluid–structure interaction is equal to the one between the moving plate and the substrate. Known are also $l = 200$ μm and $w = 100$ μm.

Problem 3.25

A plate is supported by two identical end springs and vibrates at 50,000 Hz parallel to the substrate. The area of the plate is 40,000 μm^2. Knowing the penetration depth is 80 μm, the Q-factor owing to above-the-plate fluid–structure interaction is 5,000, find the stiffness of the spring.

Problem 3.26

The losses due to friction with the fluid above the plate are 0.8 of the losses generated by air friction between the plate and the substrate. Considering the first-order slip boundary conditions, find the dynamic viscosity knowing the constant gap $z_0 = 15$ μm, vibration frequency $f = 65{,}000$ Hz, free molecular path $\lambda = 20$ μm, and plate area $A = 20{,}000$ μm^2.

Problem 3.27

A constant rectangular cross-section microcantilever of given length l, cross-sectional dimensions w and t, mass density ρ, specific heat c, coefficient of thermal expansion α, period T, frequency ω, and elastic modulus of elasticity E vibrates in vacuum. The thermal losses are monitored by means of the Q-factor Q, which is determined experimentally. Calculate the thermal conductivity k of the microcantilever material.

Problem 3.28

A 5 μm thick plate vibrates against the substrate at 100,000 Hz and T = 300 K. The properties of the plate material are: $\alpha = 3.5 \times 10^{-6}$ K^{-1}, κ = 1,500 W/(m × K), c = 700 J/(kg × K), ρ = 2300 kg/m^3, E = 1.65 GPa. Knowing the total quality factor is Q = 130,000 and the elastic support stiffness is k = 4 N/m, calculate the damping coefficient.

Problem 3.29

The Q-factor of a silicon trapezoid microresonator corresponding to defect motion is 8,000. Knowing the relaxation period is 2×10^{-13} s and the activation energy is 2 eV, as well as the microresonator's dimensions (length 200 μm, thickness 2 μm, base width 50 μm, and tip width 20 μm), determine the equivalent viscous damping ratio.

Problem 3.30

A rectangular microcantilever 300 μm long, 50 μm wide, and 2 μm thick, vibrates in air against the substrate at 16,000 Hz with an initial gap of 12 μm. The total losses due to squeeze-film damping and anchor losses are expressed by a Q-factor of 20,000. Evaluate the substrate thickness. The dynamic viscosity is $\mu = 1.8 \times 10^{-5}$ N-s/m^2.

References

1. W.T. Thomson, *Theory of Vibrations with Applications*, Third Edition, Prentice Hall, Englewood Cliffs, 1988.
2. J.J. Blech, On isothermal squeeze films, Journal of Lubrication Technology, 105, 1983, pp. 615–620.
3. T. Veijola, T. Tinttunen, H. Nieminen, V. Ermolov, T. Ryhanen, Gas damping model for a RF MEM switch and its dynamic characteristics, IEEE MTT-S International Microwave Symposium Digest, 2, 2002, pp. 1213–1216.
4. L. Zhang, D. Cho, H. Shiraishi, W. Trimmer, Squeeze film damping in microelectromechanical systems, ASME Micromechanical Systems, Dynamic Systems Measurements and Control, 40, 1992, pp. 149–160.
5. R.G. Christian, The theory of oscillating-vane vacuum gauges, Vacuum, 16, 1966, pp. 149–160.
6. Zs. Kadar, W. Kindt, A. Bossche, J. Mollinger, Quality factor of torsional resonators in the low-pressure region, Sensors and Actuators A, 53, 1996, pp. 299–303.

7. M. Bao, H. Yang, H. Yin, Y. Sun, Energy transfer model for squeeze-film damping in low vacuum, Journal of Micromechanics and Microengineering, 12, 2002, pp. 341–346.
8. S. Hutcherson, W. Ye, On the squeeze-film damping of microresonators in the free-molecular regime, Journal of Micromechanics and Microengineering, 14, 2004, pp. 1726–1733.
9. P.J. Polikarpov, S.F. Borisov, A. Kleyn, J.-P. Taran, Normal momentum transfer study by a dynamic technique, Journal of Applied Mechanics and Technical Physics, 44, 2003, pp. 298–303.
10. R. B. Darling, C. Hivick, J. Xu, Compact analytical models for squeeze film damping with arbitrary venting conditions, Transducers ’97 International Conference on Solid State Sensors and Actuators, 2, 1997, pp. 1113–1116.
11. W. Dotzel, T. Gessner, R. Hahn, C. Kaufmann, K. Kehr, S. Kurth, J. Mehner, Silicon mirrors and micromirror arrays for spatial laser beam modulation, Transducers ’97 International Conference on Solid State Sensors and Actuators, 1, 1997, pp. 81–84.
12 F. Pan, J. Kubby, E. Peeters, A.T. Tran, Squeeze film damping effect on the dynamic response of a MEMS torsion mirror, Journal of Micromechanics and Microengineering, 8, 1998, pp. 200–208.
13. M. Bao, Y. Sun, Y. Huang, Squeeze-film air damping of a torsion mirror at a finite tilting angle, Journal of Micromechanics and Microengineering, 16 (11), 2006, pp. 2330–2335.
14. T. Veijola, A. Pursula, P. Raback, Extending the valability of squeezed-film damper models with elongation of surface dimensions, Journal of Micromechanics and Microengineering, 15 (9), 2005, pp. 1624–1636.
15. N. Lobontiu, E. Garcia, Mechanics of Microelectromechanical Systems, Kluwer Academic Press, New York, 2004.
16. M. Bao, H. Yang, Y. Sun, Y. Wang, Squeeze-film air damping of thick hole plate, Sensors and Actuators A, 108, 2003, pp. 212–217.
17. M. Bao, H. Yang, Y. Sun, P.J. French, Modified Reynolds’ equation and analytical analysis of squeeze-film air damping of perforated structures, Journal of Micromechanics and Microengineering, 13, 2003, pp. 795–800.
18. S.S. Mohite, H. Kesari, V.R. Sonti, R. Pratap, Analytical solutions for the stiffness and damping coefficients of squeeze films in MEMS devices with perforated back plates, Journal of Micromechanics and Microengineering, 15, 2005, pp. 2083–2092.
19. L.D. Landau, E.M. Lifshitz, Fluid Mechanics, Pergamon, London, 1959.
20. T. Veijola, M. Turowski, Compact damping for laterally moving microstructures with gas rarefaction effects, Journal of Microelectromechanical Systems, 10 (2), 2001, pp. 263–273.
21. P.K. Kundu, Fluid Mechanics, Academic Press, San Diego, 1990.
22. A. Burgdorfer, The influence of the mean free path on the performance of hydrodynamic gas lubricated bearings, Journal of Basic Engineering, 81, 1959, pp. 94–99.
23. A. Beskok, G.E. Karniadakis, Simulation of heat and momentum transfer in complex microgeometries, Journal of Thermophysics and Heat Transfer, 8 (4), 1994, pp. 647–655.
24. A. Beskok, G.E. Karniadakis, W. Trimmer, Rarefaction and compressibility effects in gas microflows, Journal of Fluids Engineering, 118, 1996, pp. 448–456.
25. P. Bahukudumbi, J.H. Park, A. Beskok, A unified engineering model for steady and quasi-steady shear-driven gas microflows, Microscale Thermophysical Engineering, 7, 2003, pp. 291–315.
26. J.H. Park, P. Bahukudumbi, A. Beskok, Rarefaction effects on shear driven oscillatory gas flows: a direct simulation Monte Carlo study in the entire Knudsen regime, Physics of Fluids, 16 (2), 2004, pp. 317–330.
27. M.N. Kogan, Rarefied Gas Dynamics, Plenum, New York, 1969.
28. C. Cercignani, C.D. Pagani, Variational approach to boundary-value problems in kinetic theory, The Physics of Fluids, 9, 1966, pp. 1167–1173.

29. T.W. Roszhart, The effect of thermoelastic internal friction on the Q of micromachined silicon resonators, Technical Digest on Solid-State Sensor and Actuator Workshop, 1990, pp. 13–16.
30. C. Zener, Elasticity and Anelasticity of Metals, University of Chicago Press, Chicago, 1948.
31. R. Lifshitz, M.L. Roukes, Thermoelastic damping in micro and nanomechanical systems, Physical Review B, 61 (8), 2000, pp. 5600–5609.
32. D.A. Czaplewski, J.P. Sullivan, T.A. Friedmann, D.W. Carr, B.E. Keeler, J.R. Wendt, Mechanical dissipation in tetrahedral amorphous carbon, Journal of Applied Physics, 97, 2005, pp. 023517, 1–023517, 10.
33. V. B. Braginski, V.P. Mitrofanov, V.I. Panov, Systems with Small Dissipation, University of Chicago Press, Chicago, 1985.
34. L. Burakowsky, D.L. Preston, An analytical model of the Gruneisen parameter at all densities, Journal of Physical Chemistry and Solids, 65, 2004, pp. 1581–1595.
35. R.E. Mihailovich, N.C. MacDonald, Dissipation measurements of vacuum operated single-crystal silicon microresonators, Sensors and Actuators A, 50, 1995, pp. 199–207.
36. Y.-H Park, K.C. Park, High-fidelity modeling of MEMS resonators – Part I: Anchor loss mechanisms through substrate, Journal of Microelectromechanical Systems, 13 (2), 2004, pp. 238–247.
37. H. Osaka, K. Itao, S. Kuroda, Damping characteristics of beam-shaped micro-oscillators, Sensors and Actuators A, 49, 1995, pp. 87–95.
38. Z. Hao, A. Erbil, F. Ayazi, An analytical model for support loss in micromachined beam resonators with in-plane flexural vibrations, Sensors and Actuators A, 109, 2003, pp. 156–164.
39. D. Photiadis, J.A. Judge, Attachment losses of high Q oscillators, Applied Physics Letters, 85 (3), 2004, pp. 482–484.
40. K.Y. Yasumura, T.D. Stowe, E.M. Chow. T. Pfafman, T.W. Kenny, B.C. Stipe, D. Rugar, Quality factors in micron- and submicron-thick cantilevers, Journal of Microelectromechanical Systems, 9 (1), 2000, pp. 117–125.